pH- RESPONSIVE DEXTRAN GATED FUNCTIONIZED MESOPOROUS SILICA FOR DRUG DELIVERY

A THESIS PRESENTED TO THE DEPARTMENT OF MATERIAL SCIENCE AND ENGINEERING

AFRICAN UNIVERSITY OF SCIENCE AND TECHNOLOGY, ABUJA

IN PARTIAL FULFILLMENT OF THE REQUIREMENTS FOR THE AWARD OF THE DEGREE OF

MASTER OF SCIENCE

BY

YUSUF OLATUNJI WAIDI

SUPERVISOR: PROF. WINSTON OLUWOLE SOBOYEJO

CO-SUPERVISOR: DR. OLUSHOLA ODUSANYA

JULY, 2019

pH- RESPONSIVE DEXTRAN GATED FUNCTIONIZED MESOPOROUS SILICA FOR DRUG DELIVERY

BY

YUSUF OLATUNJI WAIDI

Approved by: _____

Prof. Winston Oluwole Sobeyejo

(Supervisor)

Approved by: _____

Dr. Olushola Odusanya

(Co-supervisor)

Approved by: _____

Prof. Azikiwe Peter Onwualu

(Head of Department, Materials Science and Engineering)

Approved by: _____

Prof. C. E. Chidume

(Chief Academic Officer)

CERTIFICATION

This is to certify that the thesis titled "***pH- Responsive Dextran Gated Functionized Mesoporous Silica for Drug Delivery***" submitted to the Department of Materials Science and Engineering, African University of Science and Technology (AUST), Abuja, Nigeria for the award of the Master's degree is a record of original research carried out by ***Yusuf, Olatunji Waidi.***

DEDICATION

To Allah, from whom everything comes, I am more than grateful for Your mercy and favour, all of which I do not deserve.

To my irreplaceable Mom and Dad, I certainly would not have achieved this without your uncompromising love, support and encouragement. I wish it was ever possible to repay you.

To my siblings, you've always been exceptional and I wouldn't have wished for any better siblings.

To my friends and colleagues, having you has been fun all through, the courage I derived from you couldn't possibly be got from somewhere else. You all have driven this success from the very beginning, thumbs up!

ABSTRACT

Mesoporous materials have generated a lot of interest over the past few decades owing to their wide range of applications in catalysis, separation, drug delivery, sensors, adsorption, photonics, nanodevices etc. To realise such applications, it is necessary to regulate the transport of molecules through the mesochannels which resulted in a surge of interest to manipulate the pore size, surface charge and philicity. The current work presents the results of an experimental study of a technique whereby synthesized mesoporous silica were hetero-functionalized with carboxylic acid and propylamine functional groups in certain proportions giving rise to pH-dependent charge reversal surfaces. A cationic dye (cargo) was loaded into the mesoporous silica at basic pH utilizing the electrostatic attractions between dye molecules and anionic surfaces. The loaded cargo could be quantitatively released by decreasing the pH to the acidic range. Further, by employing dextran as a pore gating system, we were able to demonstrate an efficient system of cargo release system. There was a huge difference between the release at pH for both Mesoporous silica spheres functionalized with amine and succinic anhydride (MCM-Z) and Mesoporous silica spheres functionalized with amine and succinic anhydride Dextran capped (MCM-ZD). But for MCM-Z, the release at pH 5 was higher than that of MCM-ZD as expected. The % weight release of both room temperature and temperature controlled *in vitro* environments were similar. For the first time, we were able to functionalize a mesoporous nano silica with succinic anhydride using 1,4-dioxane as solvent in a particular way to have such unique properties for the required application.

ACKNOWLEDGEMENTS

During my MSc., I have been helped by a large number of people, to whom I will always be grateful. Firstly, my soul shall praise the living God. He alone answered my prayers. I am glad with what God has done for me in my life, most especially seeing me through my MSc program in African University of Science and Technology. I cannot imagine how success could come my way if my God was not by my side.

It is a great pleasure to sincerely appreciate my supervisor, *Prof Winston Oluwole Soboyejo*, a distinguished professor at Worcester Polytechnic Institute, USA, and former president of African University of Science and Technology. Beyond just being a supervisor, you were a father to me. The inspiration I drew from you will forever impact my life. I am profoundly appreciative. And also my sincere gratitude goes to my co-supervisor, *Dr. Shola Odusanya* for his ever ready assistance.

It is a great pleasure to thank our collaborator, *Prof. M. Eswaramoorthy (JNCASR)* for fruitful collaborations. And also my special thanks to my labmates, the "NanoCat" group members at JNCASR: *Ms. Suchi Smita Biswas, Ms. Soumita Chakraborty, Mr. Momin Ahamed, Mr. Arunava Saha, Ms. Divya Bhutani, Ms. Surishi Vashishth, Ms. Nijita Mathew, Mr. Abhishek, Dr. Mehraj Ud Din Sheikh, Dr. Monoj Kumar Barman,* for their cooperation, useful discussions and for creating a friendly atmosphere in the lab. Working with them was a real pleasure. Not to forget to mention the main man behind the success; *Dr. K. P. Sonu* for his full assistance.

My sincere gratitude also goes to the Pan Africa Materials Institute (PAMI) through funding from World Bank for providing sponsorship for my M.Sc. studies. Thanks a whole lot for working to lift Africa from the dungeon of illiteracy, poverty and backwardness.

Thanks and appreciation goes to all Ph.D. and M.Sc. materials students of AUST for your support and attention. You were always at my service when I need you.

TABLE OF CONTENTS

Contents **Pages**

LIST OF FIGURES

CHAPTER ONE

1.0 INTRODUCTION

1.1 Background and Introduction

Over the past few decades, huge advances have been made in synthesis of ordered porous solids with controlled pore size, shape and regularity of the pores [1–3]. Ordered mesoporous silica is exceptional among them due to their high surface area, ease of synthesis and chemical modifications, high thermal stability and bio-compatibility [4–8]. In most cases, mesoporous silica is synthesized via organic-inorganic assembly of amphiphilic surfactants and silicate species (produced by base or acid catalysed hydrolysis of silane precursors, tetraalkoxysilane). The amphiphilic surfactants is responsible for structure directing agents or templates. Finally, the solid mesoporous silica can be obtained by removing the template (via calcination or ion exchange or simple washing) after the condensation of silicates species around the superstructures formed by surfactant molecules (template) [9,10].

Surface engineering in the context of mesoporous silica is basically associated with working and controlling the parameters like pore structure, pore philicity and surface charge. Due to the fact that, these parameters define the mass transport through the mesopores, it is necessary to optimise them for their applications in drug delivery[8,11–14], sensing[15], catalysis[16,17], bio-mimetic channels[18,19] among others. So, in this study, we explored a unique way of functionalizing the mesoporous silica nanoparticles and incorporated a suitable pore gating system to aides the release efficiency at a particular pH.

1.2 Scope of the Present Investigation

In this research, we demonstrated a unique technique to achieve dextran gate-controlled release of cargo from mesoporous silica by surface engineered the material to obtain a suitable surface charge. The generic strategy used a pH-dependent charge reversal mesoporous silica having the capability to control the release of charged cargos from the channels, in response to pH change but the case that has been reported for this system only worked at a very lower pH, which is not suitable for cancer therapy of pH-5. The hetero-functionalized mesoporous silica consisting of carboxylic acid and propylamine functional groups in certain proportion give rise to pH-dependent charge reversal surface (*i.e.* cationic surface at acidic pH due to protonation of amine groups and anionic surface at basic pH due to deprotonation of carboxylic acid groups). The cationic dye (cargo) was loaded into the mesoporous silica at basic pH utilizing the electrostatic attractions between dye molecules and anionic surfaces. The loaded cargo could be quantitatively released by decreasing the pH to the acidic range. Further, by employing dextran as a pore gating system, and thus, therefore demonstrate an efficient system of cargo release system.

CHAPTER TWO

2.0 LITERATURE REVIEW

2.1 Pore Gating

Pore gating is an important strategy to control the movement of cargo molecules from the pores of the mesoporous silica to the solution and vice versa, in response to pre-programmed stimulus (Figure 2.1)[20]. In this approach, the entrapped cargo molecules are physically blocked from releasing via pore blocking agents (polymers[21–23], cyclodextrins[24,25], nanoparticles[26–29]etc. attached at the entrance of the nanochannels. Once an appropriate stimulus is applied, the pore blocking agent is removed from the mesoporous silica to release the cargo molecules. The gated mesoporous silica nanodevices have demonstrated the potential of achieving pre-designed functions by means of mass transport regulation. The most studied applications of such systems are related to the drug delivery[30] and smart catalysis [31,32].

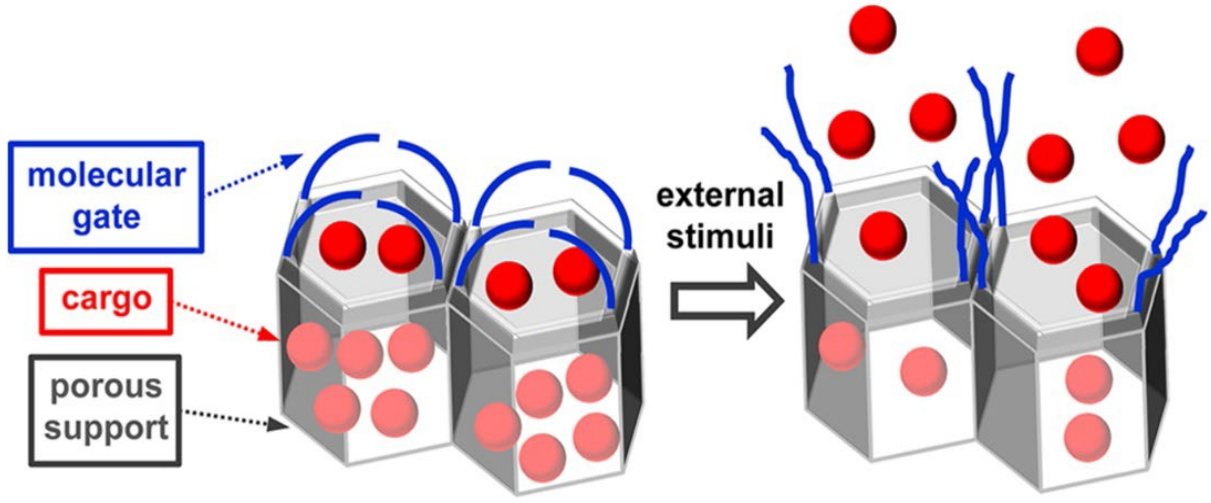

Figure 2.1. *Schematic representation of a gated material for on-command controlled release* [20].

2.2 Molecular Entities for Pore Gating.

Various molecular motifs such as (bio)-polymers[22],[33],[34], DNA aptamers[35,36], lipids3[37,38], coumarin[39], thymine[40] etc. have been successfully used as effective pore blocking agents at mesoporous silica surface. For instance, Kleitz *et al*., designed and synthesised a β-lactoglobulin functionalized mesoporous silica for pH dependent release of ibuprofen (Figure 2.2).[23] At pH < 5 β-lactoglobulin on mesoporous silica surface undergoes a gelation process, leading to the--formation of intermolecular hydrogen-bonded β-sheet. This conformational change is associated with lower solubility of the β-lactoglobulin in acidic media, resulting in a pH dependent "gel-shell" around the mesoporous silica. This gel will prevent the drug molecule release from the mesopores. At pH > 5, β-lactoglobulin becomes permeable, allowing the drug to get released.

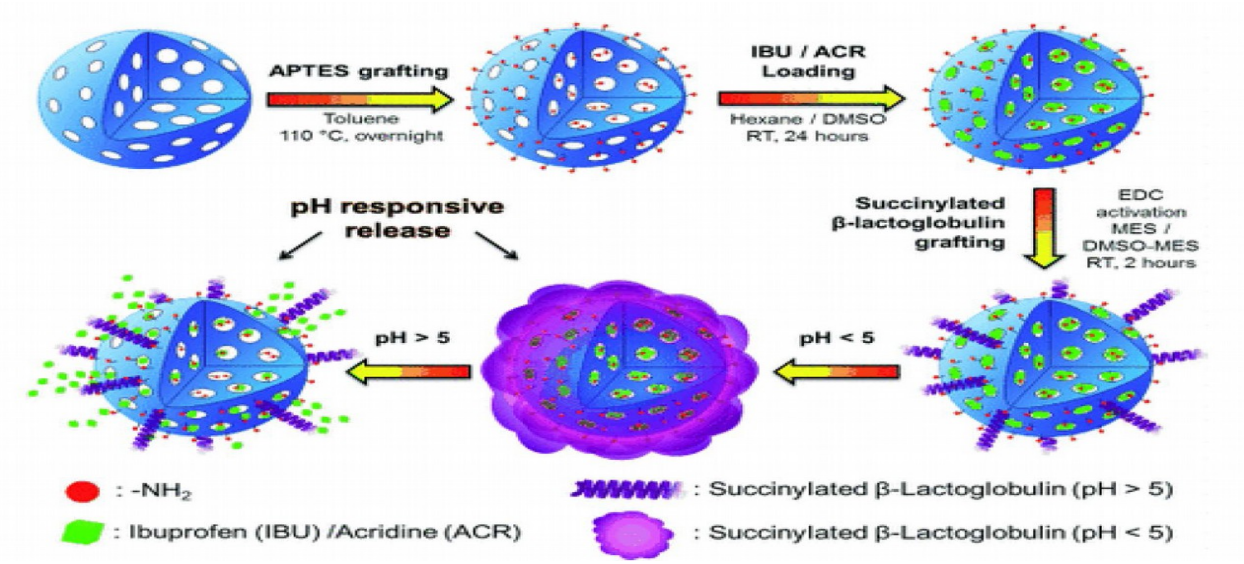

Figure 2.2. *Schematic representation of the post-grafting, bio-functionalization, and pH-responsive release of drug or dye from basic pH sensitive MNPs* [23].

Lately, He and co-workers synthesised a controlled release system in which polymer containing coumarin moieties was used to gate the mesoporous silica (Figure 2.3) [20],[39]. Therefore, the irradiation with 365 nm UV light leads to the formation of coumarin dimers which cross-link the polymer and effectively block the entrapped cargo molecules. Notwithstanding, when the hybrid was irradiated at 264 nm UV light, the coumarin moieties returned to the monomer form, therefore, open up the pores that leads to the release of entrapped cargo.

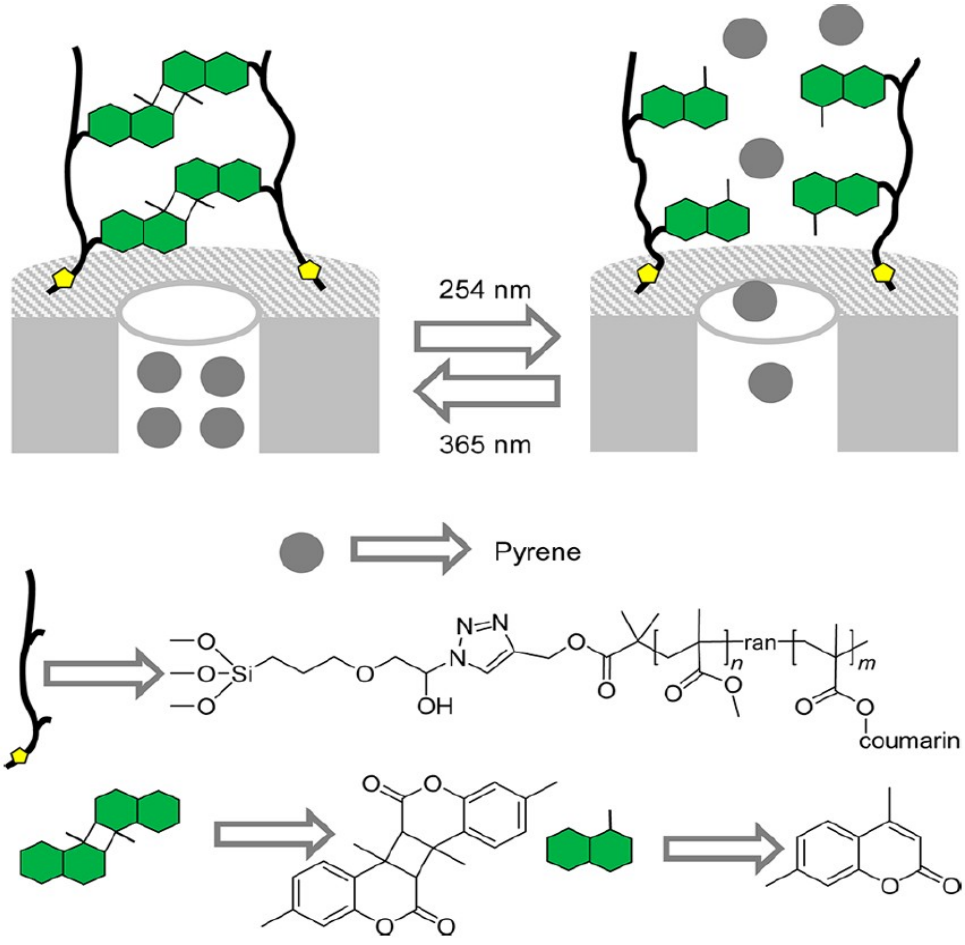

Figure 2.3. *Gated MSNs loaded with pyrene and capped with a methyl methacrylate and 7-(2-methacryloyloxy)-4 methylcoumarin copolymer. Pyrene was released upon irradiation at 254 nm* [20].

2.3 Supramolecular Entities for Pore Gating

Supramolecular motifs like cyclo-dextrins[41–43], cucurbitural[24,44], crown-ethers[45,46] and pillararenes[47,48] possessing molecular dimensions are of the order of pore size of mesoporous silica (2-3 nm) have also been utilized as pore gating agents. For instance, azobenzene which is known to have a strong binding affinity with β-cyclodextrin in its *trans* form have been used widely on mesoporous silica surface as a light responsive supramolecular motif. Stoddart, Zink, and co-workers prepared mesoporous silica nanoparticles (MSNs) with outer surface modified with (E)-4-((4-(benzylcarbamoyl) phenyl)diazenyl)benzoic acid derivative [20,41]. The azo-modified MSN were capped with β-cyclodextrins (β-CDs) through the formation of inclusion complexes with *trans* isomer of the grafted azobenzenes. Cargo delivery was triggered by irradiation with a laser light of 351 nm that switch the azobenzene from *trans* isomer to *cis* form as shown in (Figure 2.4). β-cyclodextrins were unable to thread to the stack (*cis*-form of azobenzene) as a consequence, the entrapped cargo (RhB) molecules were released.

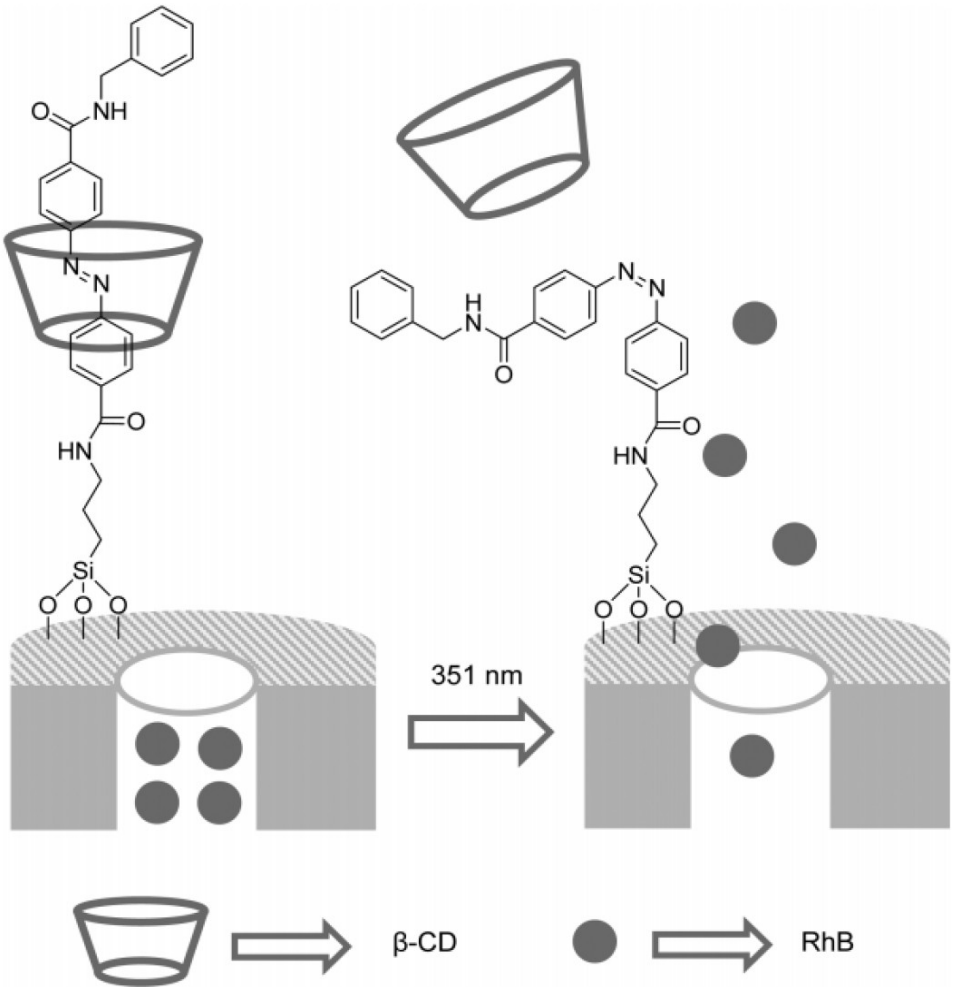

Figure 2.4. *Azobenzene functionalized mesoporous silica loaded with Rh B and capped with β-CD. Rh B was released upon irradiation at 351 nm* [20].

2.4 Nanoparticles for Pore Gating

Several nanoparticles of diameter around 3 nm have been utilized to effectively block the pores of mesoporous silica. These nanoparticles are typically attached to the external surface by stimuli responsive covalent linkages such as imide bonds, disulfide bonds, boronic ester bonds etc. Couple of the nanoparticles utilized for this purpose are gold nanoparticles [26,49,50], CdS nanoparticles[51], Fe_3O_4 nanoparticles[28,29] etc. For example, Lin and co-workers immobilized cadmium sulfide (CdS) nanoparticles on mesoporous silica surface utilizing

disulfide linkages (Figure 2.5) [51] which were then used to block the encapsulated drug molecules -vancomycin and ATP. As soon as disulfide bond-reducing molecules like dithiothreitol was used as a trigger, encapsulated drug molecules were released from the mesopores.

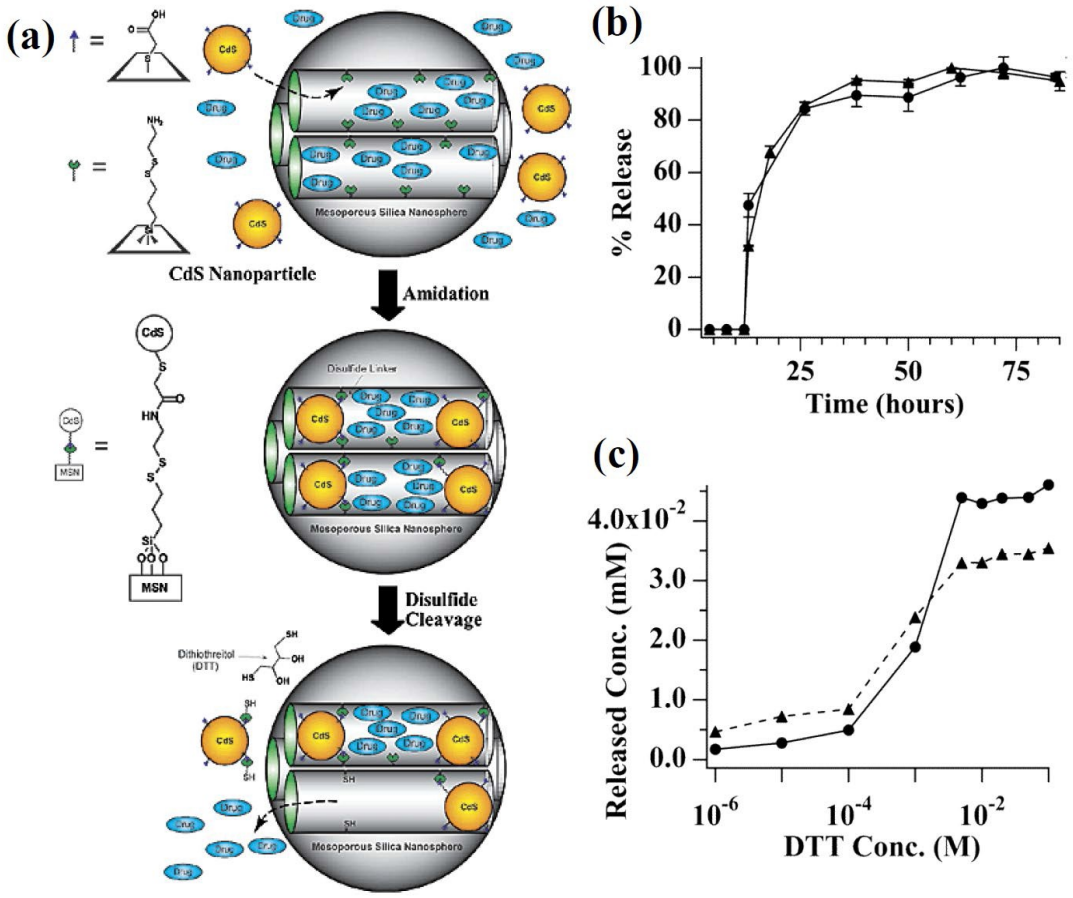

Figure 2.5. *(a) Schematic representation of CdS nanoparticle-capped MSN-based drug delivery system. The controlled release mechanism of the system is based on chemical reduction of the disulfide linkage between the CdS caps and the MSN hosts. (b) The DTT-induced release profiles of Vancomycin (dotted) and ATP (tringle) from the CdS-capped MSN system. (DTT: dithiothreitol) over time. (c) The DTT concentration-dependent releases of Vancomycin (dotted) and ATP (tringle)* [51].

2.5 Surface Charge Modulation

The movement of charged molecules through mesoporous silica is governed predominantly by surface charge on the pore surface due to the fact that size of these pores are comparable to the Debye length [52]. Hence, the electrostatic potential does not decay to the bulk values even at the centre of the pore [53,54]. Thus, create asymmetry of ion distribution inside the nanochannels/nanopores (counter-ion in nanochannels is enriched while the co-ion concentration decreased) due to the electrostatic interactions between ions and the charges of the nanopores (Figure 2.6). The asymmetric ion-distribution within nanopores makes them permselective with respect to ion transport by favouring the transport of counter ion [55]. This permselective nature of mesoporous silica nanochannels have been examined for various applications such as sensing[18], fabrication of abiotic nanochannels[56], charge mediated delivery[57], electrochemical energy conversion[58] etc.

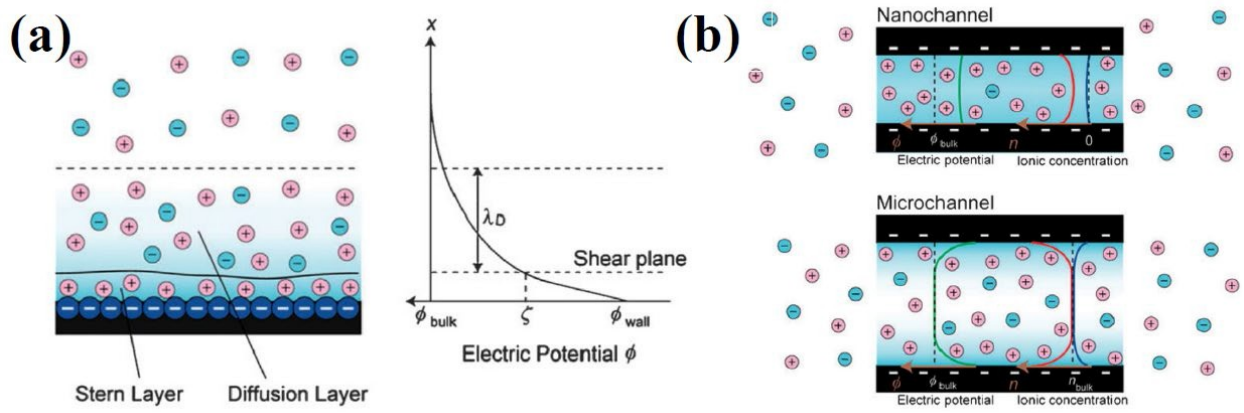

Figure 2.6. *(a) Schematics showing the distribution of ions in a flat surface. Distribution of electric potential as a function of distance from the surface. The electric potential decay exponentially within Debye length. (b) The ion distribution in a nanochannel is almost unipolar in nature because its dimensions are smaller than the Debye length. In the case of*

nanochannels the electric potential even at the centre of the channel is influenced by the surface charge. Note that the concentration of the cations are higher in the nanochannels compared to anions. However, in the case of microchannels where the diameter is higher than that of Debye length, the electric potential rapidly drops to its bulk value and hence it shows similar concentrations of anions and cations within it [55].

2.6 Surface Charge Modulation and Charge Reversal in Nanopores

Surface charge in nanochannels have been mostly modulated by attaching certain charge bearing group(s) such as quaternium ammonium[57], viologen groups[59] etc. For example, Omar Azzaroni *et al.* have used phosphate-bearing polymer brushes that shows pH responsive charging to modulate the surface charge inside the pores of SBA-16 thin films and therefore modulate their perm selective properties (Figure 2.7) [60]. The pKa of these phosphate groups are 7.7 and 4.5, hence, below 4.5 the phosphate groups are unionized giving a non-selective ion transport. Although, at pH 5 the surface becomes negatively charged owing to the ionization of phosphate groups and the channels show strong cation selective transport.

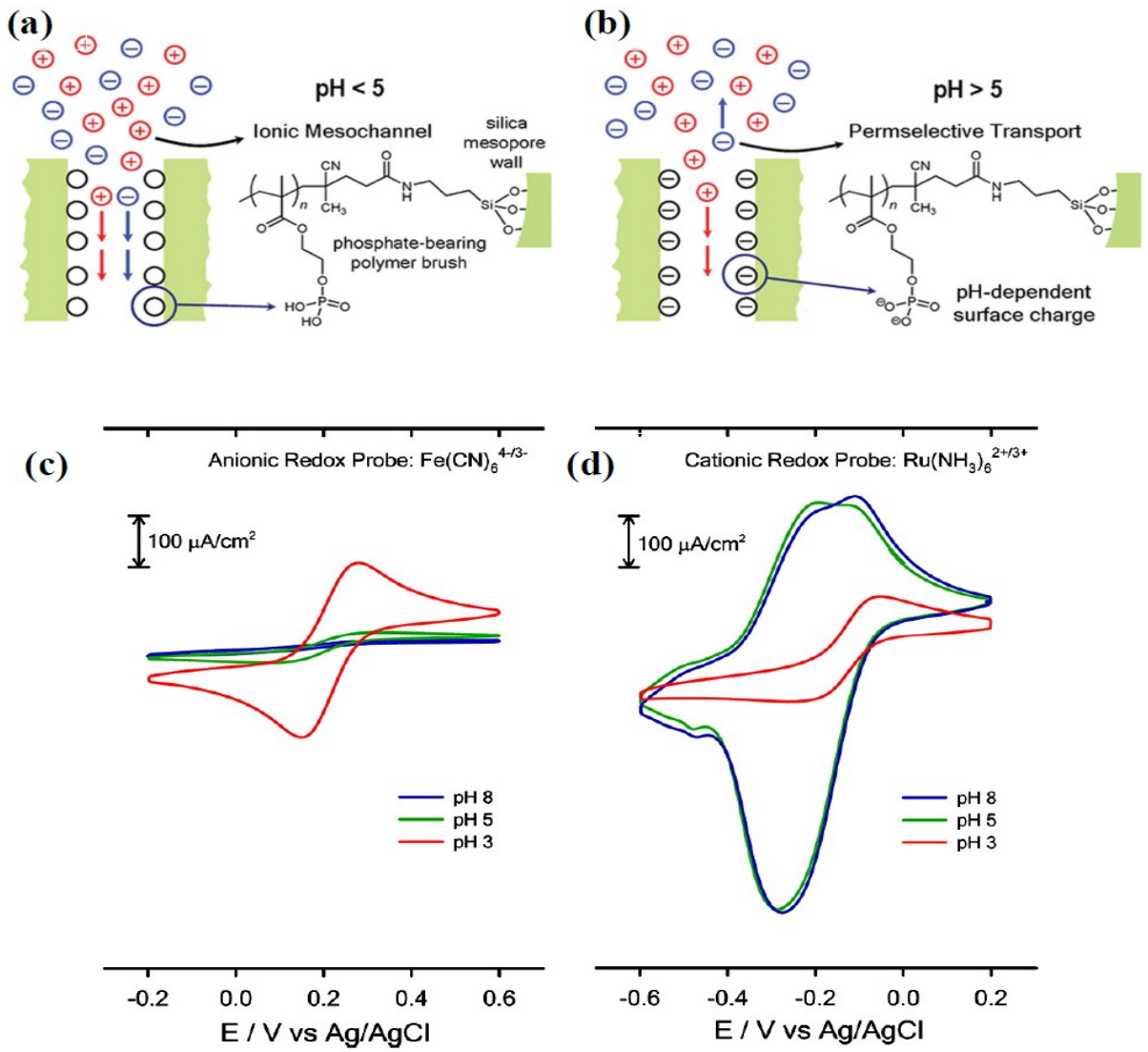

Figure 2.7. *Schematic representation of the inner environment of the phosphate-bearing polymer brush attached mesoporous silica film. (a) In the case of pH <5, the phosphate groups are protonated and the nanochannels show no perm selectivity. (b) For pH >5, the ionization of phosphate groups give rise to negative surface charge inside the channels therefore they show strong cation selective transport. Comparative cyclic voltammograms displaying the molecular transport through PMEP-modified mesoporous thin films as a function of pH using (c) Fe(CN)6* $^{3-}$ *as an anionic redox probe and (d) Ru(NH3)6* $^{3+}$ *as a cationic redox probe* [60].

In addition, it is possible to switch the surface charge of nanochannels from one state to other by functionalizing them with molecules capable of switching the charge between positive and negative in response to various stimuli such as pH,[61–63] light,[64–66] redox[67] etc. (a stimuli responsive charge reversal). Thus, therefore give rise to switchable ion transport which is important for various applications. Harry L. Anderson *et al.* examined a pH responsive charge reversal surface by attaching aminodicarboxylic acid units to fused porous silica surfaces (Figure 2.8) [68]. The anionic and cationic dye adsorption capabilities of these surface was explored to identify the charge reversal. At the acidic pH of around 1, the surface became positively charged due to the protonation of tertiary amine groups. At this ionic state, the surface indicates enhanced anionic dye adsorption through electrostatic attraction. On the other hand, the surface becomes negatively charged at pH 7 owing to the ionization of carboxylic acid groups. At this pH the surface shows enhanced adsorption for cationic dyes.

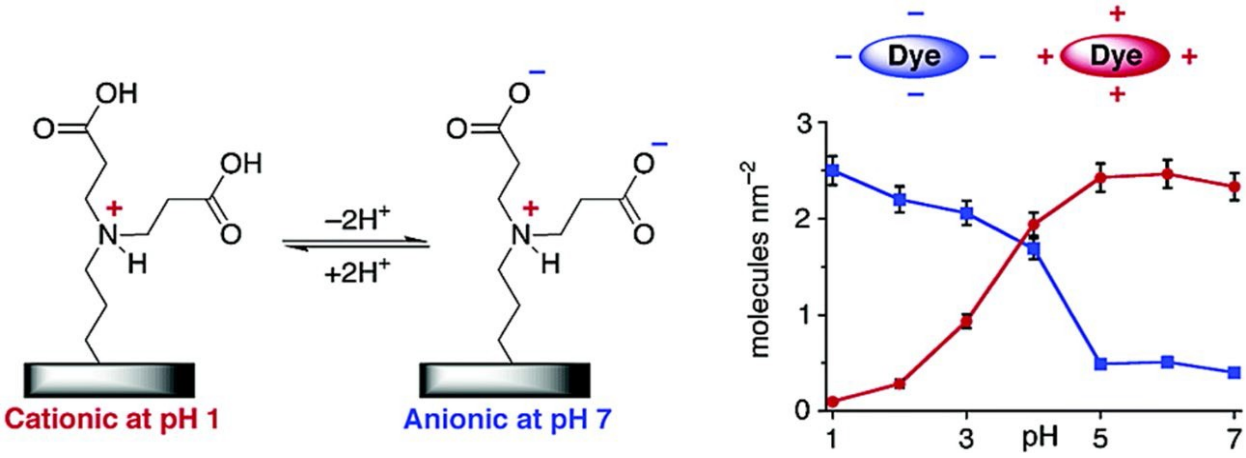

Figure 2.8. *Schematic representation of fused porous silica surfaces designed for the pH responsive charge reversal. The pH dependent cationic and anionic dye adsorption to this surface* [68].

Moreover, it is also possible to achieve charge reversal through hetero-functionalization strategy. In this approach two or more types of molecules are anchored to the surface to synergistically accomplish certain total surface charge [69,70]. Therefore, the magnitude of the total charge can be easily modulated via controlling the ration of charge bearing molecules. For instance, Pavan *et al.* have demonstrated a hetero-functionalization approach to establish a dual stimuli responsive (pH and glucose) charge reversal mesoporous surface [71]. This was achieved by functionalizing mesoporous silica with propylamine and phenylboronic acid groups in a 1:1 ratio (Figure 2.9). At pH 3, the surface is highly positive due to the protonation of amine groups and it can be switched to negative upon increasing the pH to 9 where the phenylboronic acid groups start to ionize due to the binding of hydroxyl ions. Further, the surface ionization can be modulated through addition of glucose which binds to phenylboronic acid and lower the pKa of the ionization equilibrium. Therefore the negative surface could readily be achieved at much lower pH (ca. 7.4)

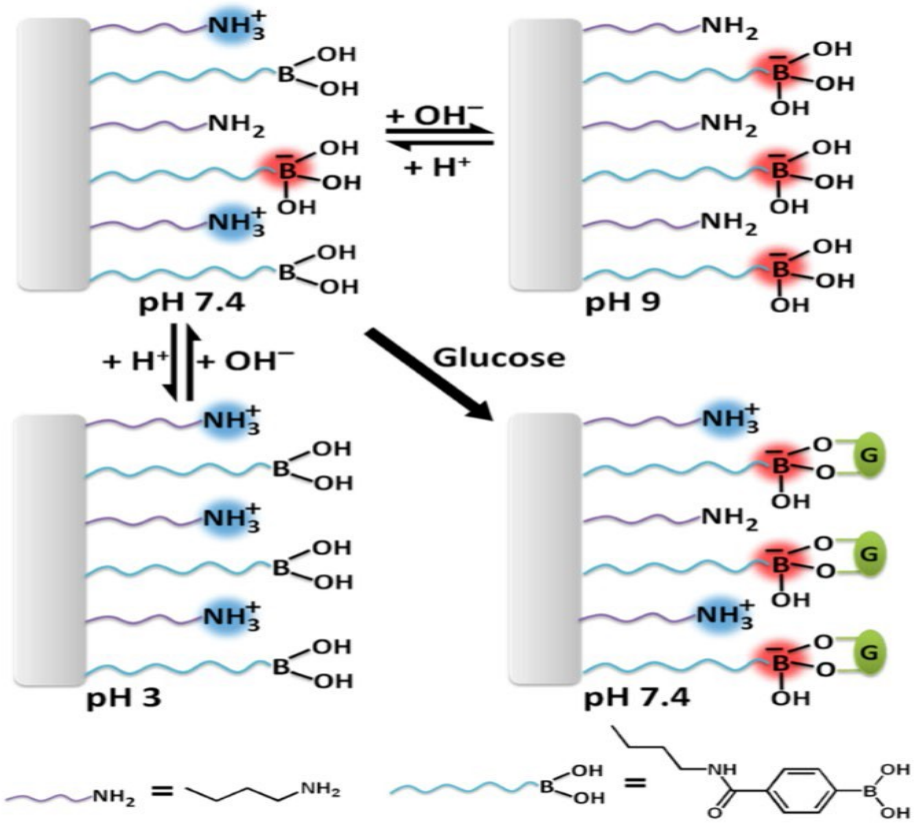

Figure 2.9. *Schematic representation of dual mode charge reversal in a hetero-functionalized mesoporous silica* [71].

2.7 pH-Responsive Drug-Delivery Systems

pH values in various segments of the gastrointestinal tract, different organs, tissues, and cellular compartments are different. For instance, the pH values vary in a wide range from the stomach (pH 1.5–3.5) and small intestine (pH 5.5–6.8) to the colon (6.4–7.0) [72]. The pH values in tumors and inflammatory tissues are lower than those in blood and normal tissues (7.4), and the acidic cellular environments exhibit even lower pH values (e.g., endosomes (pH 5.5–6.0) and lysosomes (pH ~4.5–5.0) [73]. Therefore, the difference in the pH value of different organs, tissues and cellular compartments may provide a suitable physiological stimulus for pH-responsive drug delivery. The strongly pH-dependent drug release profile of the drug-delivery

system is an ideal platform for targeted drug delivery because the drug release is inhibited during systemic circulation at the physiological pH value of 7.4 and the drug is released only in the acidic environment of cancer cells.

Recently, there have been many reports of organic-polymer-based pH-responsive drug-delivery systems in the literature; nevertheless, more and more papers have been published in recent years regarding inorganic, and in particular inorganic/organic composite, pH-responsive drug-delivery systems due to their advantages in terms of biocompatibility, thermal stability, variety, and control of morphology, size, and structure. And also, there are an increasing number of papers published regarding inorganic pH-responsive drug-delivery systems in recent years due to their advantages in terms of thermal stability, biocompatibility, rich variety, and easy control of morphology, size, and structure. Most of the reported inorganic materials as pH-responsive drug carriers include Au nanostructures, carbon based nanostructures, mesoporous silica, and calcium phosphate-based nanostructured materials. Of these inorganic materials, calcium phosphate-based nanostructured materials are very promising as excellent pH-responsive drug carriers due to their high biocompatibility and pH sensitivity; calcium phosphates can dissolve to form Ca^{2+} and PO_4^{3-} ions in acidic environments, which are fundamental constituents in vivo. Gu *et al.*[74] reported a drug-delivery system based on single walled carbon nanotubes loaded with Doxorubicin (DOX) by employing a hydrazine bond. It was observed that the DOX-loaded carbon nanotubes could be favourably taken up by HepG2 tumor cells and release DOX intracellularly. In comparism with the DOX-loaded carbon nanotubes, the carbon nanotubes /hydrazinobenzoic acid/DOX drug-delivery system had higher DOX loading and prolonged DOX release. Zhu *et al.*[75] studied mesoporous carbon nanospheres (-90 nm) as a drug carrier for pH-dependent DOX release. By effective passive and active targeting, mesoporous carbon

nanospheres could be internalized into HeLa cells, in which the carried DOX could be favourably released in the acidic microenvironment of the tumors.

Li *et al*.[76] prepared mesoporous silica hollow microspheres with diameters in the range of 100 to 500 nm and wall thicknesses of approximately 50 nm by employing cetyltrimethylammonium bromide by the microfluidization technique, and the as-prepared mesoporous silica hollow microspheres were effective for drug loading and pH-responsive drug release. Ma *et al*.[77] prepared mesoporous silica hollow spheres with perpendicular nanochannels that connected to internal hollow cores as the carrier for DOX/siRNA co-delivery; and folic acid-conjugated polyethyleneimine was coated on mesoporous silica hollow spheres under neutral conditions to block the mesopores and halt the loaded drugs from leaking. Folic acid served as the targeting ligand and enabled the co-delivery system to selectively bind with and enter into the target cancer cells.

In summary, surface engineering possibilities of mesoporous silica with suitable functionalities to precisely regulate the mass transport has broadened the scope of their applications in various fields such as adsorption, sensing, separation, photonics, drug delivery etc. Therefore the control of molecular transport through the mesopores can be achieved by physically blocking the pore and by manipulating parameters such as pore size, pore philicity and pore surface charge through surface functionalization.

CHAPTER THREE

3.0 METHODOLOGY

3.1 Materials and Reagents.

[3-(2-Aminoethylamino)propyl] trimethoxysilane (AEAPS), tetraethoxysilane (TEOS), tetramethylamonium hydroxide (25 wt % in methanol, TMAH), and dextran (Mr 6000 and 100000) were all purchased from Sigma−Aldrich and used as received. 1-ethyl-3-(3-(dimethylamino)propyl)carbodiimide hydrochloride (EDC) was purchased from TCI Chemicals and used as received. Cetyltrimethylammonium bromide (CTAB) was purchased from Alfa Aesar. N-hydroxysuccinimide (NHS) was purchased from Fluka. And succinic anhydride was purchased from Merck.

3.2 Synthesis of MCM-41.

Mesoporous silica nanoparticles (MCM-41) were synthesized by following a previously reported procedure [78]. In a typical synthesis, 1.0 g (2.74 mmol) of hexadecyltrimethyl-ammonium bromide (CTAB) and 0.28 g of NaOH were dissolved in 480 mL of water under stirring and the temperature was raised to 80°C. 5 ml (22.4 mmol) of tetraethyl orthosilicate (TEOS) was added dropwise to the reaction mixture and stirred for 2 h at 80 °C. The white solid product was centrifuged, washed thoroughly with water followed by ethanol, and dried in an oven for overnight. The surfactant (CTAB) was removed by refluxing it for 6 h in acidic ethanol solution (50 mL EtOH containing 0.5 mL concentrated HCl (37 %)). The precipitate was thoroughly washed with water and ethanol. The as-synthesized MCM-41 was dried under high vacuum.

3.3 Synthesis of MCM-N.

1.0 g of surfactant-free MCM-41 (1.0 g) and 1.0 mL (5.67 mmol) of (3 aminopropyl)triethoxysilane (APTES) were added to 80 mL anhydrous toluene and ultra-sonicated to get a homogenous dispersion. The mixture was refluxed along with stirring under N_2 atmosphere for 24 h. The reaction mixture was centrifuged and the precipitate was washed thoroughly with toluene, hexane followed by ethanol, finally dried under high vacuum at 80 °C for 6 h.

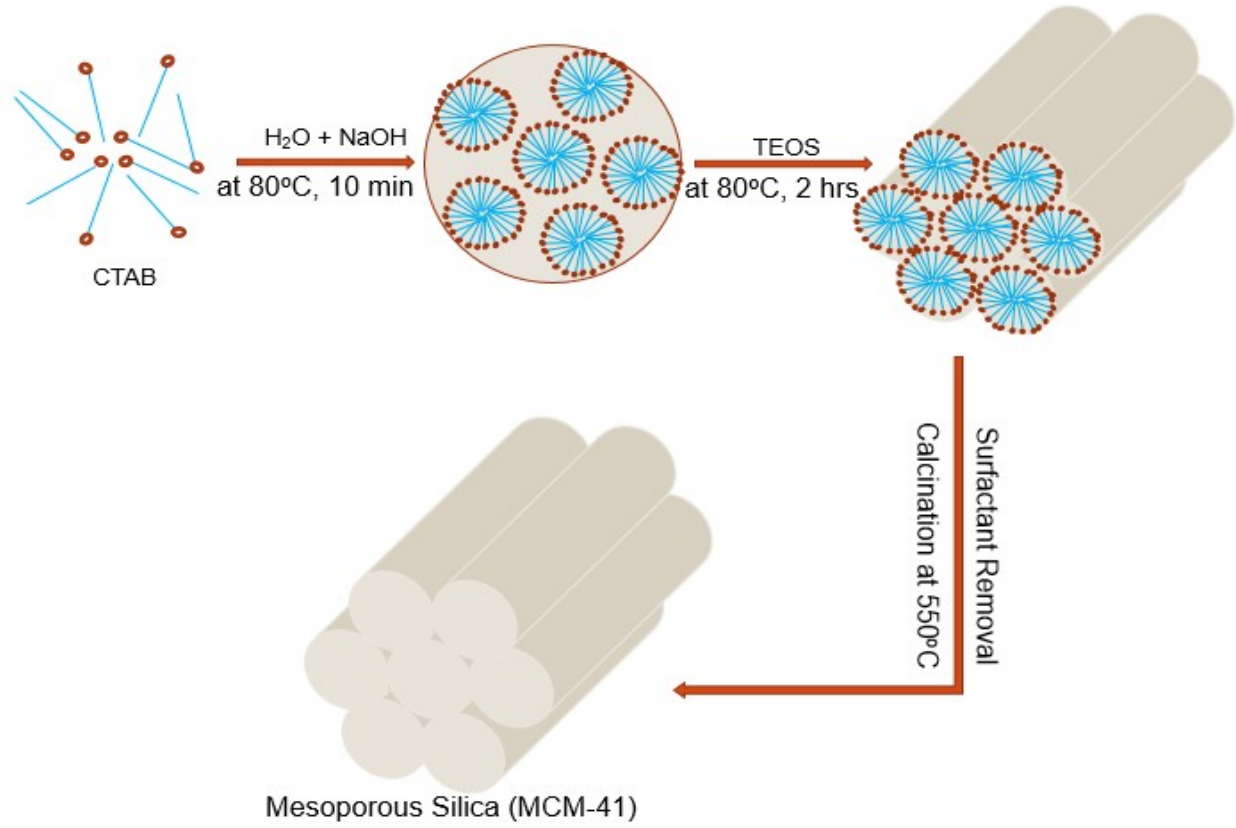

Figure 3.1. *Schematic showing the Diagrammatic representation of the formation mechanism of MCM-41.*

3.4 Synthesis of MCM-Z.

0.5 g of MCM-N was dispersed in 25 mL 1,4-dioxane and ultra-sonicated for 5 minutes. To this dispersion, a solution of 20 mg of succinic anhydride (0.2 mmol) in 12.5 mL of 1,4-dioxane was added under stirring. This mixture was heated at 80°C for 10 minutes. The resultant product was centrifuged, and washed thoroughly with water followed by ethanol, and dried in an oven for overnight.

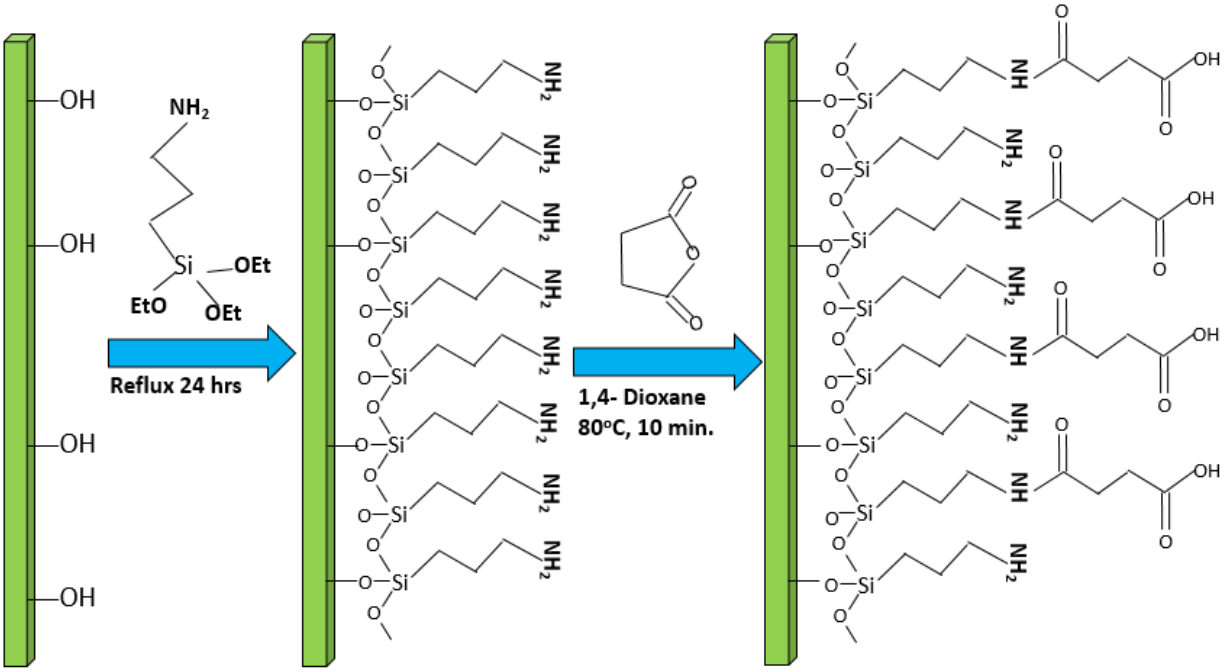

Figure 3.2. *Schematic showing the synthetic strategy for functionalization of MCM nanochannels to create pH-responsive hetero functionalized MCM-Z nanochannels.*

3.5 Calculation of Quantitative Coverage of Functionalization.

For MCM-N:

The TGA provided the weight of overall organic functionalization of MCM-N (19.4 %)

Amount of propylamine groups present in MCM-N = 1.94 mmol/g (From TGA measurements).

Number of molecules of propylamine = 1.94 mmol x NA /g

Where NA = 6.02 x 10^{23}

= 1.16788 x 10^{21} molecules/g

Surface area of MCM-41 = 965 m^2/g

= 987 x 10^{18} nm^2/g

Number of propylamine groups per nm^2 = 1.16788 x 10^{21} molecules / 987 x 10^{18} nm^2

= **1.183 molecules / nm^2**

For MCM-Z:

The TGA provided the weight of overall organic functionalization of MCM-Z (11.3 %)

Amount of carboxylic acid groups present in MCM-Z = 1.13 mmol/g

Number of molecules of carboxylic acid moieties = 1.13 mmol x NA /g

= 6.803 x 10^{20} molecules/g

Number of carboxylic acid groups per nm^2 = 6.803 x 10^{20} molecules / 987 x 10^{18} nm^2

= **0.69 molecules/ nm^2**

3.6 Zeta potential measurements.

A dispersion of MCM-41, MCM-N or MCM-Z having a concentration of 0.5 mg/mL in the respective buffers was used for the zeta potential measurements. The measurements were carried out in a Zetasizer Nano ZS (Malvern, UK) employing a 532 nm laser at a backscattering

angle of 173°. The temperature was always kept at 25°C with the help of inbuilt thermostat in Zetasizer Nano ZS.

3.7 Preparation of samples for Nitrogen adsorption-desorption.

The samples were degassed at 85 °C for 12 h under high vacuum and then nitrogen adsorption-desorption experiments were carried out at -196 °C.

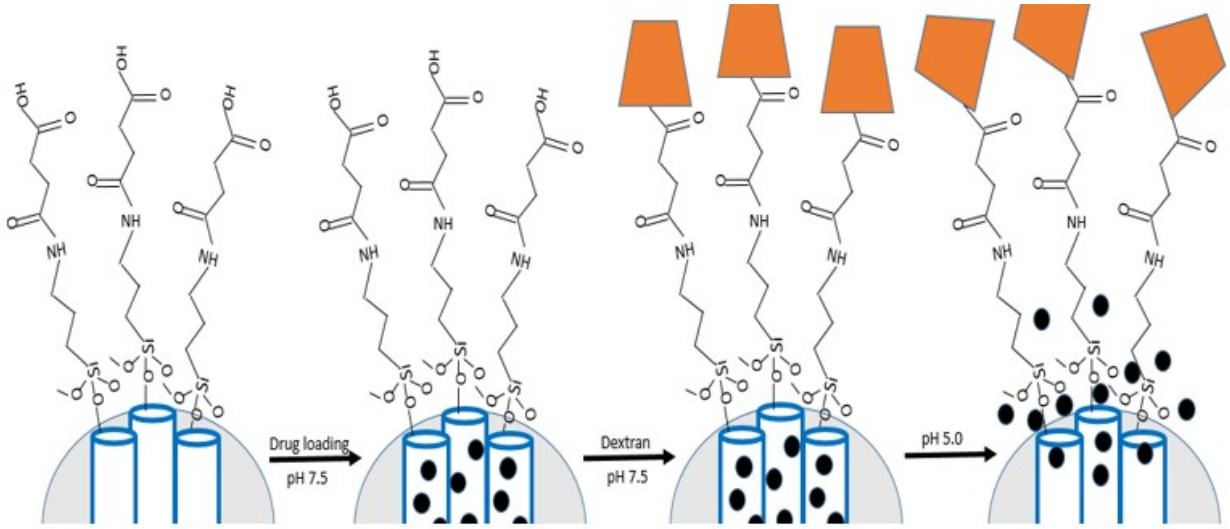

Figure 3.3*. Schematic illustration of drug loading at pH 7.5, coating it with dextran at pH 7.5 and release at pH 5.*

3.8 CV^+ dye loading to MCM-Z

Loading of CV^+ into the mesoporous channels of MCM-Z was achieved as follows. 5 mg of MCM-Z was dispersed in 1.95 mL pH 8.0 Tris-HCl buffer (10 mM). To this, a 0.05 mL of CV^+ solution (stock concentration of 0.5 mM) was added and the resultant dispersion was mixed well. The suspension was stirred for 12 h at room temperature for dye loading. Then, the dispersion was, washed extensively with Tris-HCl buffer solution to remove physisorbed dye. The collected CV^+ loaded MCM-Z and the supernatant was subjected to UV-Vis spectroscopy to calculate the loading amount.

3.9 Preparation of Dextran Functionalized (MCM-Z dextran)

Drug loaded MCM-Z particles were dispersed in PBS buffer of pH 7.4, mixed with 4 mL aqueous solution of dextran (25 mg/mL) and kept under stirring condition for 3 h. Next, particles were separated, washed with PBS buffer of pH 7.4 for the removal of unbound dextrans. Resultant drug loaded MCM-Z was redispersed in aqueous solution for further application.

3.10 pH-dependent CV^+ release from MCM-Z and MCM-ZD

The CV^+-loaded MCM-Z (5 mg) and MCM-ZD (5 mg) was dispersed in 1 mL buffer (10 mM) of respective pH separately. The aliquots (0.2 mL) were taken at regular intervals of 1 hour and at room temperature, 37 ^oC, 41 ^oC and 47 ^oC to monitor the CV^+ release and the volume of the sample was adjusted with respective buffer. The amount of CV^+ released was monitored by UV-visible absorption spectroscopy.

3.11 General characterization and equipment.

Powder XRD patterns were recorded using Bruker-D8 diffractometer using Cu Kα radiation, (=1.54 Å, Step size: 0.02, Current: 30 mA and Voltage: 40 kV). The N_2 adsorption studies at -196 °C were performed on an Autosorb-1C (Quantachrome corp.). The samples were outgassed at 80 °C for 12 h under high vacuum before the analysis. The specific surface areas (SSA) were calculated according to the BET method using the Quantachrome software (ASiQwin). Ultrahigh purity gases (99.9995%) were used for all experiments. Thermogravimetric analysis experiments were performed using Mettler Toledo 850 from 30 °C to 1000 °C in oxygen stream with a heating rate of 10 °C/min. FT-IR spectra were recorded on a Bruker IFS 66v/S spectrometer. Electronic absorption spectra were recorded on a Perkin Elmer Lambda 900 UV-

Vis-NIR spectrometer and emission spectra were recorded on Perkin Elmer Ls 55 luminescence spectrometer. And also, zeta potential measurements and pH measurements were carried out.

CHAPTER FOUR

4.0 RESULTS AND DISCUSSION

Mesoporous silica spheres (MCM) (Figure 3.1) were synthesized following a well-known sol-gel procedure and the surface was covalently modified with (3- aminopropyl)triethoxysilane to obtain MCM-N with amine-functionalized surface. A portion of amine groups was then reacted with succinic anhydride to form MCM-Z with zwitterionic nature having carboxyl and amine groups on the nanochannel surface (Figure 3.2).

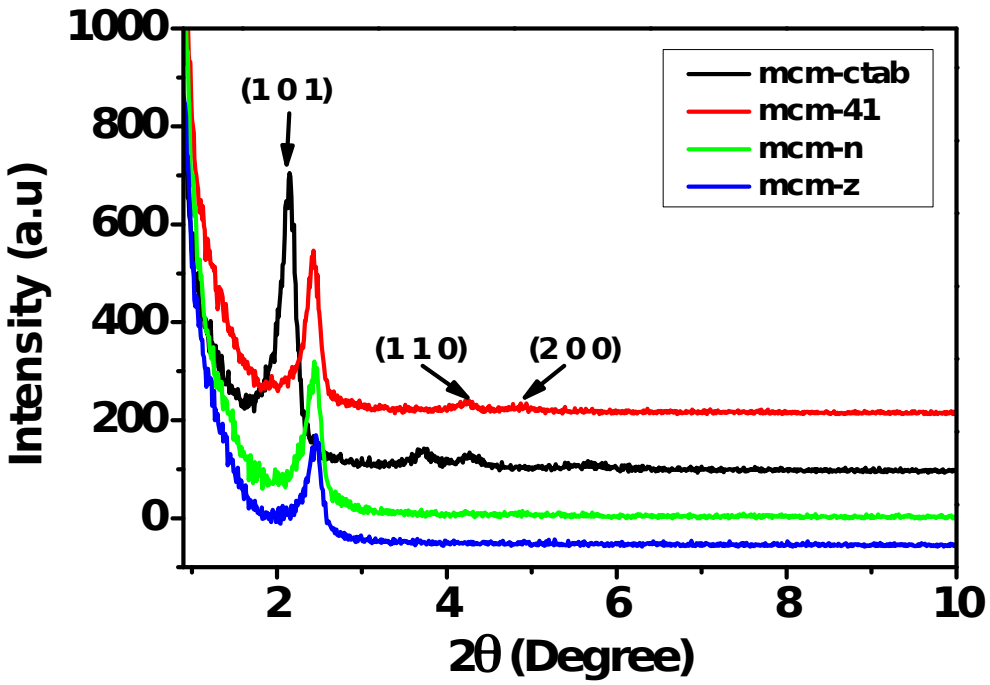

Figure 4.1. *Powder X-ray diffraction patterns of MCM-CTAB, MCM, MCM-N and MCM-Z showing retention of mesostructural ordering with the progress of functionalization. The secondary peaks [110] and [200] grow faint with functionalization.*

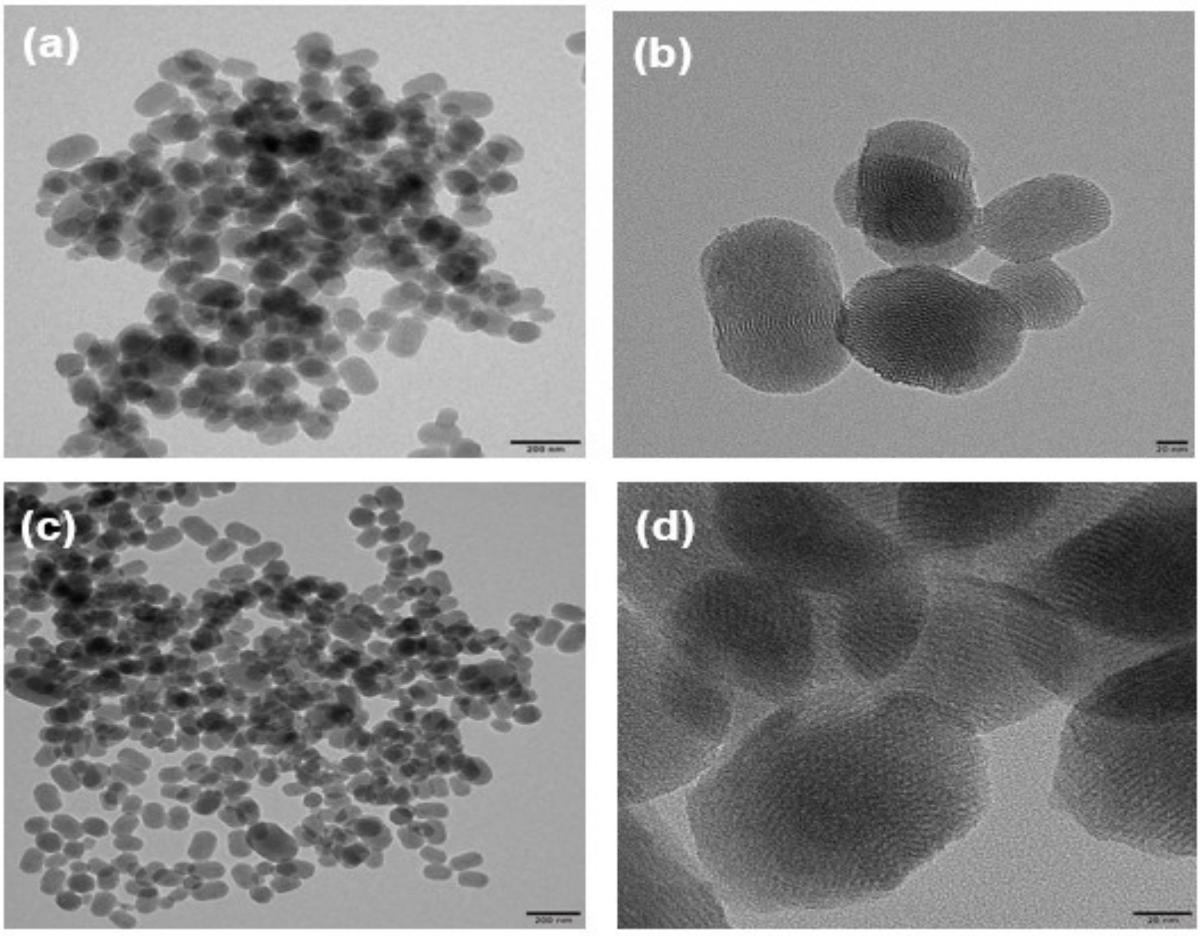

F*igure 4.2*: *TEM images showing MCM-41 nanoparticles at (a) low and, (b) high magnification. TEM images showing MCM- ZD nanoparticles at (c) low and, (b) high magnification. And TEM images of (b) MCM-41 and (d) MCM-ZD showing retention of mesostructural ordering.*

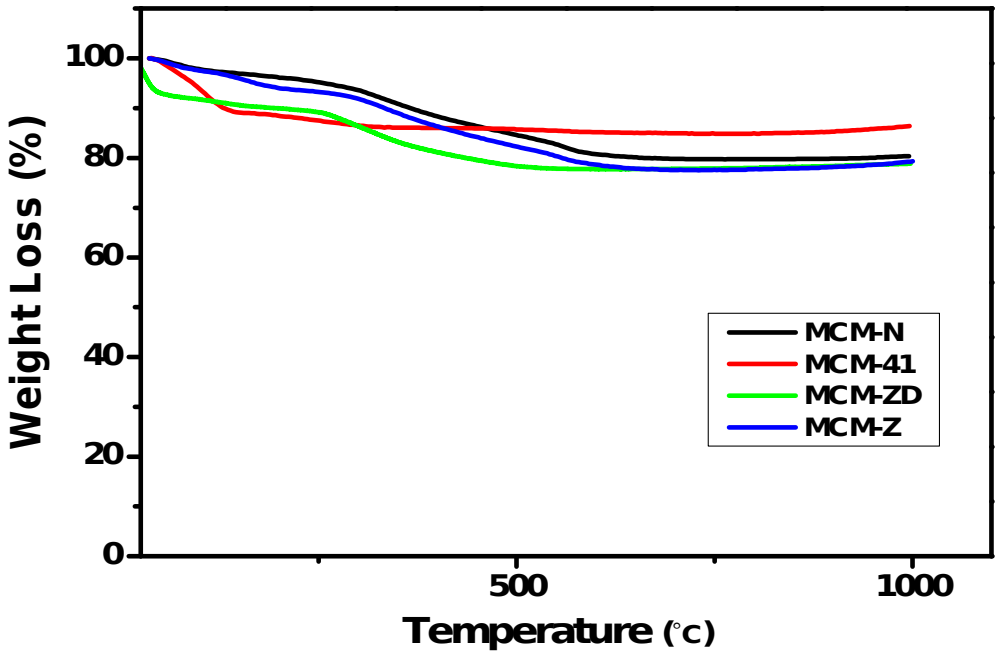

***Figure 4.3**: Thermogravimetric analysis curves of MCM-41, MCM-N, MCM-Z and MCM-ZD.*

The observation of low angle peak (at $2\theta \approx 2.2$) in the XRD patterns of MCM, MCM-N and MCM-Z suggests that the hexagonal mesostructure was retained during functionalization (Figure 4.2). Retention of mesostructure was also confirmed via transmission electron microscopy (Figure 4.2). Thermogravimetric analysis (TGA) suggested propylamine functionalization in MCM-N was around ca. 1.94 mmol g-1 (Figure. 4.3). The carboxylic acid groups (–COOH) in MCM-Z was determined to be around ca. 1.1 mmol g-1 using TGA (Figure. 4.3). Which suggest that approximately 54% of amine groups were covalently connected (via amide linkage) to carboxylic acid groups in MCM-Z.

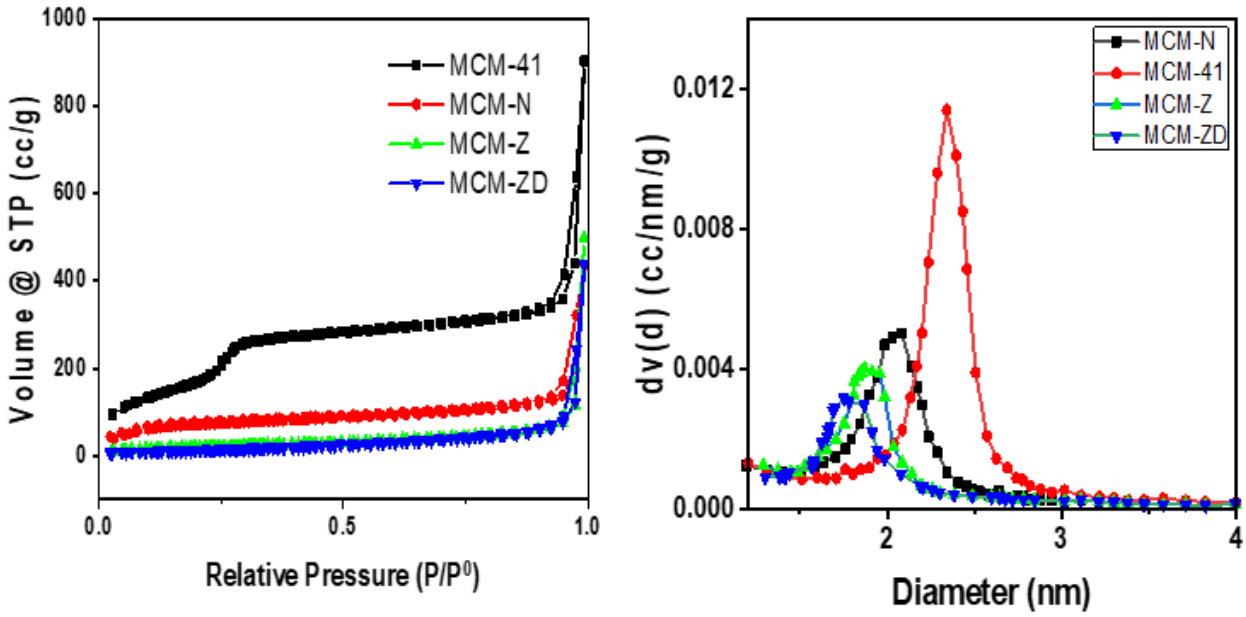

***Figure 4.4**: (a) Nitrogen adsorption-desorption isotherms and (b) Barrett-Joyner-Halenda pore size distribution curves of MCM, MCM-N, MCM-Z and MCM-ZD.*

Nitrogen adsorption-desorption analyses were carried out at -196°C to evaluate the progress of functionalization inside the nanochannels (Figure 4.4a). The Barrett−Joyner−Halenda (BJH) pore size distributions showed a gradual reduction in average pore size from ca. 2.5 nm for MCM to 2.1 nm for MCM-N which further decreased to 1.9 nm for MCM-Z and also decrease to 1.8 nm for MCM-ZD suggesting the progress of functionalization inside the nanochannels (Figure 4.4b). Furthermore, the number of propylamine groups on MCM-N was calculated to be 1.183 molecules per nm^2 area from N_2 sorption studies and TGA (see the experimental section for details). Similarly, in the case of MCM-Z, the number of carboxylic acid groups present was around 0.69 molecule per nm^2.

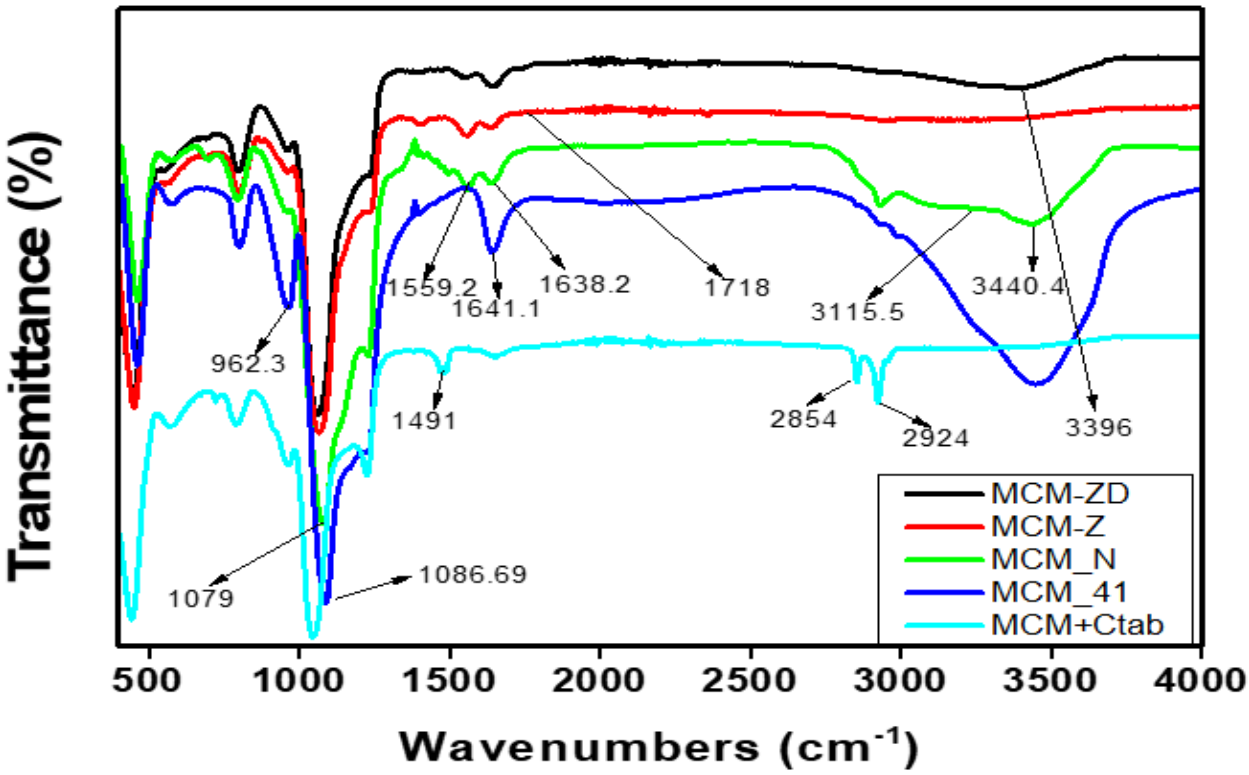

Figure 4.5: *Infra-red spectra of MCM+Ctab, MCM-41, MCM-N, MCM-Z, and MCM-ZD.*

Note: The Si-O-Si bending vibration at 460 cm-1 was used for intensity calibration.

Fourier transform infrared (FT-IR) spectra of MCM-41 with different functionalization were shown in Figure 4.5. The non-purified MCM-41(MCM-41 + CTAB) present the characteristic peaks of CTAB molecule at 2924 cm^{-1}, 2854 cm^{-1}(C H stretching vibrations) and 1491 cm^{-1}(C H deformation) [79]. Following the CTAB removal, its characteristic peaks were disappeared (Figure 4.5), which confirmed the effective purification process. The strong absorption signals of MCM-41 were shown at 1086.69 $cm^{-1}$and 962.3 cm^{-1}, mainly attributed to the stretching and asymmetric stretching of Si-O-Si bridges and skeletal vibration of the C O bonds, respectively [80]. As shown in Figure 4.5, the characteristic peak at 1559.2 cm^{-1} (stretching vibration of amide I and $-NH_2$ bending) suggested that the NH_2 groups have been coupled to the surface of MCM-41. Following modification with succinic anhydride (SA), the absorption peak at 1718

cm^{-1} (carbonyl stretch, C O, of carboxylic acid) was observed in Figure 4.5,due to the introduction of carboxyl groups deriving from succinic anhydride. And finally, the reduction of stretching at 3396 cm^{-1} was as a result of the introductions of dextran molecules.

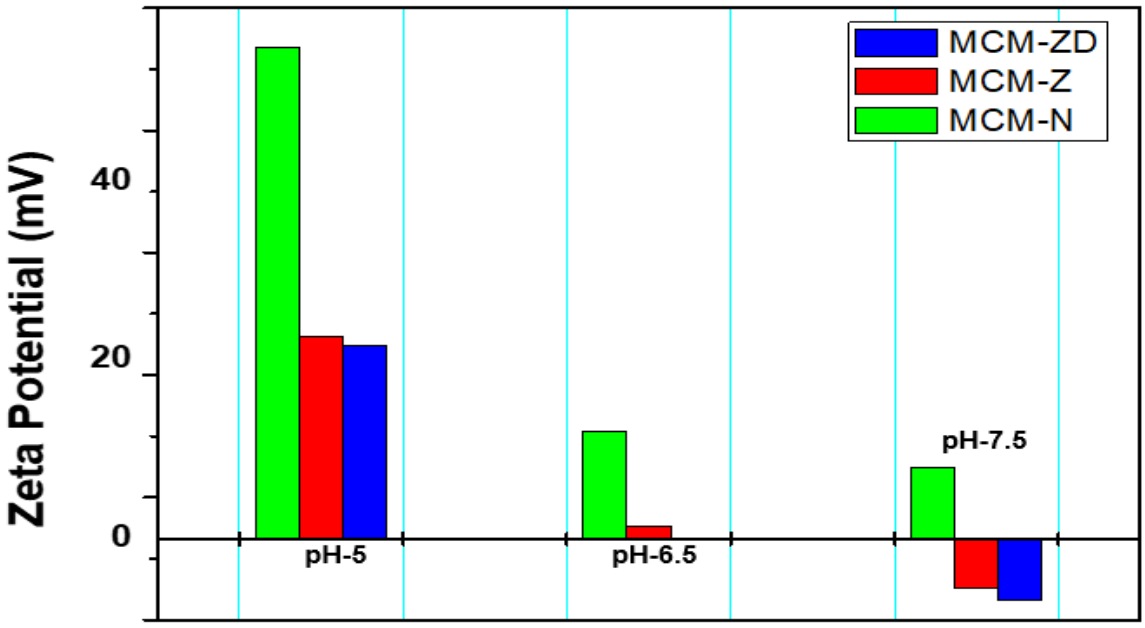

Figure 4.6: *Zeta potential distribution of MCM-N, MCM-Z and MCM-ZD at different pH*

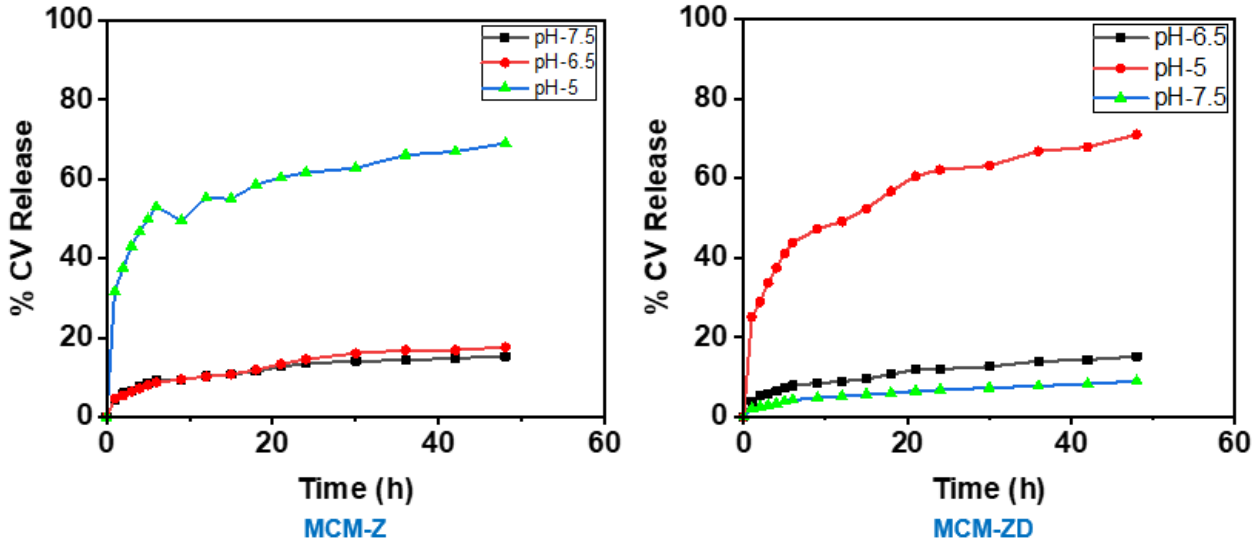

Figure 4.7: *Release profiles of CV^{+} from MCM-Z and MCM-ZD at room temperature.*

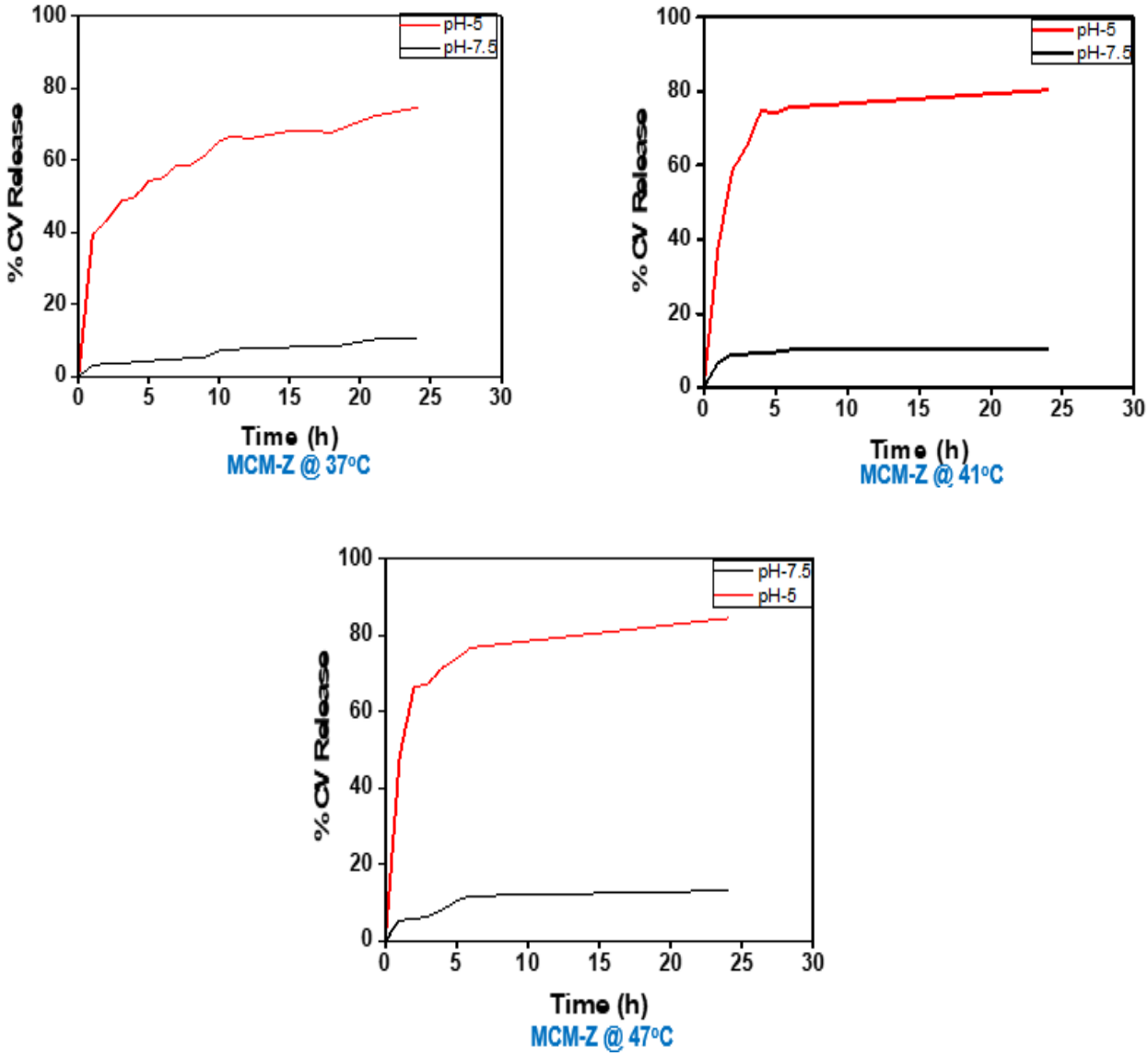

Figure 4.8: *Release profiles of CV^{+} from MCM-Z at 37℃, 41℃ and 47℃ temperature respectively.*

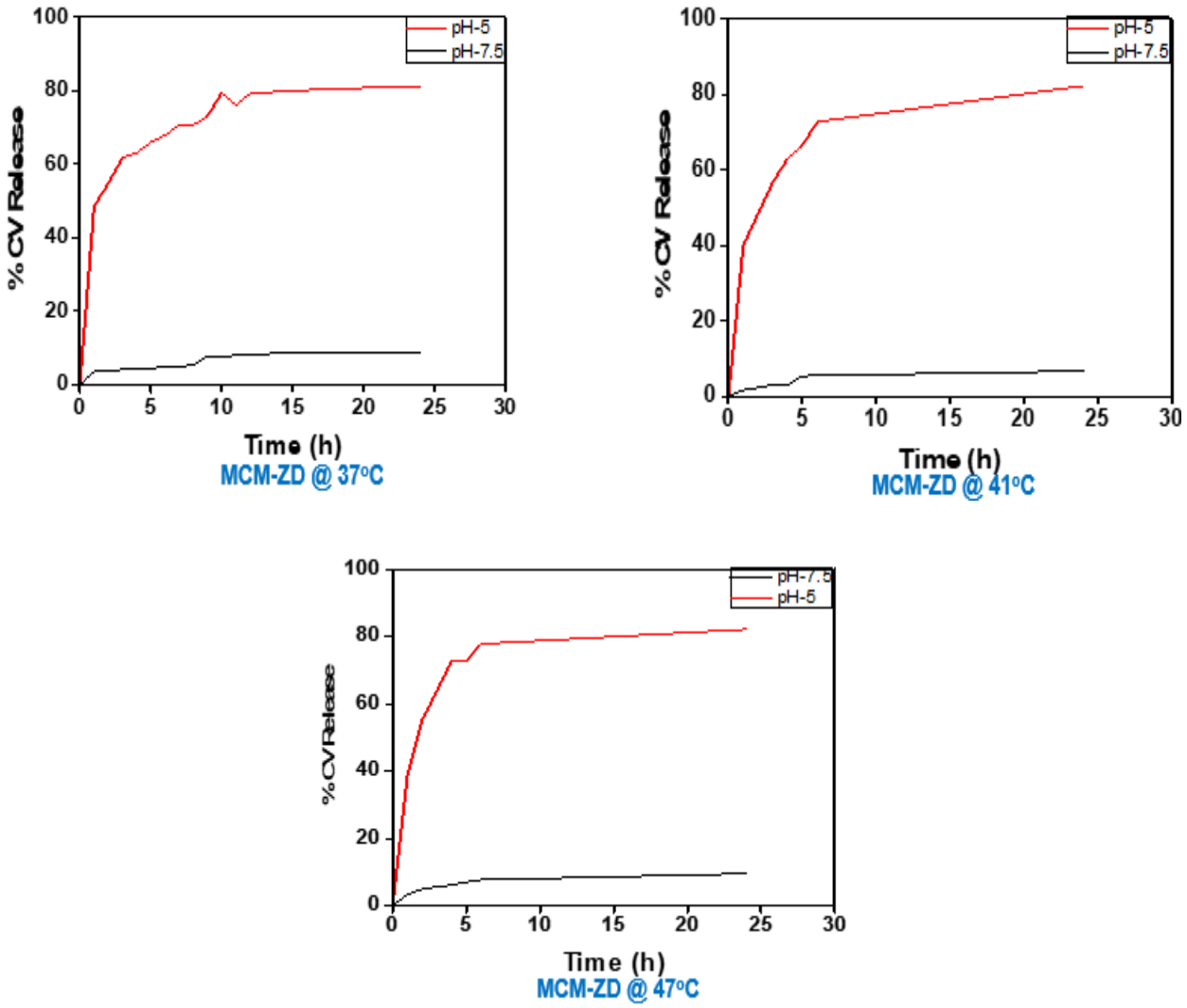

Figure 4.9: *Release profiles of CV^+ from MCM-ZD at 37℃, 41℃ and 47℃ temperature respectively.*

The successful formation of MCM-Z was also confirmed via zeta potential measurements (Figure 4.6). The zeta potential of MCM-N at pH 8 was found to be around + 30 ± 2 mV which changed to - 11 ± 1 mV for MCM-Z owing to the deprotonated carboxylic acid groups on the surface of the silica. The charge reversal of mesoporous silica (MCM-Z) was characterized though zeta potential measurements at different pH. When the pH was ca. 5.0, the surface showed a zeta potential about + 23 ± 1 mV due to protonation of amine groups. Upon increasing

the pH, the zeta potential decreased to zero at a pH of about 6.0 (isoelectric point) and further decreased to – 7± 0.5 mV at pH 7.5 due to the formation of carboxylate groups. However, the charge reversal of MCM-ZD was characterized though zeta potential measurements at different pH as well. When the pH was ca. 5.0, the surface showed a zeta potential about + 21 ± 1 mV due to bond breakage of dextran molecules and protonation of amine groups. Upon increasing the pH, the zeta potential decreased to zero at a pH of about 6.5 (isoelectric point) and further decreased to – 10± 0.5 mV at pH 7.5 due to the formation of carboxylate groups.

The nanochannels with charged surfaces are known to display charge selective transport properties associated with the surface charge-dependent gating phenomena [52] [81,82]. The CV^+ was first loaded into the MCM-Z at pH 8.5 (about 5 μmol/g loading) where the negatively charged silica surface and positively charged dye molecule attract each other via electrostatic interactions. The loaded CV^+ could be quantitatively released by carefully adjusting the surrounding pH. The pH dependent release of CV^+ from MCM-Z studied at different pH and room temperature (Figure 4.7), showed no significant release of dye at pH 7.5 owing to the strong electrostatic attraction between the silica surface and dye molecules. However, a substantial release of CV+ was observed at pH 5 owing to the electrostatic repulsion - (see the schematics in Figure 4.7). It is interesting to note that the pH-dependent release of CV+ from MCM-Z and MCM-ZD is highly quantitative in nature (Figure 4.7). The desorption response was 8 % and 9 % at pH 7.5 and 6.5 respectively for and MCM-Z, while 5 % and 8 % at pH 7.5 and 6.5 respectively for MCM-ZD. However, the CV^+ desorption from MCM-Z was significantly increased to 68 % at pH 5.0, while the CV+ desorption from MCM-ZD was significantly increased to 74 % at pH 5.0.

In addition, the pH dependent release of CV^+ from MCM-Z and MCM-ZD studied at different pH and temperatures (Figure 4.8 & 4.9), showed no significant release of dye at pH 7.5 owing to the strong electrostatic attraction between the silica surface and dye molecules. However, a substantial release of CV^+ was observed at pH 5 owing to the electrostatic repulsion - (see the schematics in (Figure 4.8 & 4.9). The desorption response was 9%, 10% and 12% at pH 7.5 for 37℃, 41℃ and 47℃ respectively for and MCM-Z, while 8%, 6% and 10% at pH 7.5 for 37℃, 41℃ and 47℃ respectively for MCM-ZD. However, the CV^+ desorption from MCM-Z was significantly increased to 78%, 81% and 83% at pH 5.0 for 37℃, 41℃ and 47℃ respectively, while the CV^+ desorption from MCM-ZD was significantly increased to 82%, 82% and 81% at pH 5.0 for 37℃, 41℃ and 47℃ respectively.

Finally, desorption conditions for both MCM-Z and MCM-ZD at different temperatures showed no significant differences in release. At 37℃, the CV^+ desorption from MCM-Z was 78%, while that of MCM-ZD was 82%. And at 41℃, it was 81% for MCM-Z and 82% for MCM-ZD. Lastly, for 47℃, the release was 83% for MCM-Z and 81% for MCM-ZD. This signifies that the release mechanism at those temperature were not temperature motivated. In essence, temperatures does not have any effect or any significant effect on the release from the nanochannel of the mesoporous silica.

CHAPTER FIVE

5.0 CONCLUSION AND FUTURE WORK

5.1 CONCLUSION

In summary, mesoporous silica was successfully synthesized and functionalized. The required Characterizations were done on the synthesized materials. Release study of the obtained materials were carried using Crystal Violet dye as a model Drug at both Room Temperature and Temperature Controlled, and also at different pH. There was a huge difference between the release at pH of 5 and 7.5 for both MCM-Z and MCM-ZD. But for MCM-Z, the release at pH 5 was high than that of MCM-ZD as expected owing to the dextran gated molecules incorporated. The % weight release for both room temperature and temperature controlled were similar. For the first time, a mesoporous nano silica spheres was functionalized with succinic anhydride using 1,4-dioxane as solvent to give such unique properties which is required for the particular application.

5.2 FUTURE WORK

The strategy presented in this work could further extended to achieve number of other pH stimuli response drug delivery system as well as expected to widen the scope of mesoporous silica based information processing. This work could be also be further investigated by experimenting the use of an anti-cancer drug. Then proceed to cell and animal work to validate the viability of the technique.

References

[1] Barton T J, Bull L M, Klemperer W G, Loy D A, McEnaney B, Misono M, Monson P A, Pez G, Schere G W, Vartuli J C and Yaghi O M 1999 Tailored porous materials *Chem. Mater.* **11** 2633–56

[2] Davis M E 2002 Ordered porous materials for emerging applications *Nature* **417** 813–21

[3] Slater A G and Cooper A I 2015 Function-led design of new porous materials *Science (80-.).* **348** 988–12

[4] Yang P, Gai S and Lin J 2012 Functionalized mesoporous silica materials for controlled drug delivery *Chem. Soc. Rev.* **41** 3679–98

[5] Rosenholm J M, Sahlgren C and Lindén M 2010 Towards multifunctional, targeted drug delivery systems using mesoporous silica nanoparticles - Opportunities & challenges *Nanoscale* **2** 1870–83

[6] Wu S H and Lin H P 2013 Synthesis of mesoporous silica nanoparticles *Chem. Soc. Rev.* **42** 3862–75

[7] Lu J, Liong M, Li Z, Zink J I and Tamanoi F 2010 Biocompatibility, biodistribution, and drug-delivery efficiency of mesoporous silica nanoparticles for cancer therapy in animals *Small* **6** 1794–805

[8] Li Z, Barnes J C, Bosoy A, Stoddart J F and Zink J I 2012 Mesoporous silica nanoparticles in biomedical applications *Chem. Soc. Rev.* **41** 2590–605

[9] Chen C Y, Li H X and Davis M E 1993 Studies on mesoporous materials. I. Synthesis and characterization of MCM-41 *Microporous Mater.* **2** 17–26

[10] Trewyn B G, Slowing I I, Giri S, Chen H T and Lin V S Y 2007 Synthesis and functionalization of a mesoporous silica nanoparticle based on the sol-gel process and applications in controlled release *Acc. Chem. Res.* **40** 846–53

[11] Slowing I I, Vivero-Escoto J L, Wu C W and Lin V S Y 2008 Mesoporous silica nanoparticles as controlled release drug delivery and gene transfection carriers *Adv. Drug Deliv. Rev.* **60** 1278–88

[12] Slowing I I, Trewyn B G, Giri S and Lin V S Y 2007 Mesoporous silica nanoparticles for drug delivery and biosensing applications *Adv. Funct. Mater.* **17** 1225–36

[13] Vallet-Regí M, Balas F and Arcos D 2007 Mesoporous materials for drug delivery *Angew. Chemie - Int. Ed.* **46** 7548–58

[14] Tang F, Li L and Chen D 2012 Mesoporous silica nanoparticles: Synthesis, biocompatibility and drug delivery *Adv. Mater.* **24** 1504–34

[15] Sancenõn F, Pascual L, Oroval M, Aznar E and Martínez-Máñez R 2015 Gated Silica Mesoporous Materials in Sensing Applications *ChemistryOpen* **4** 418–37

[16] Joo S H, Park J Y, Tsung C K, Yamada Y, Yang P and Somorjai G A 2009 Thermally stable Pt/mesoporous silica core-shell nanocatalysts for high-temperature reactions *Nat. Mater.* **8** 126–31

[17] Jiao F and Frei H 2009 Nanostructured cobalt oxide clusters in mesoporous silica as efficient oxygen-evolving catalysts *Angew. Chemie - Int. Ed.* **48** 1841–4

[18] Paquin F, Rivnay J, Salleo A, Stingelin N and Silva C 2015 Multi-phase semicrystalline microstructures drive exciton dissociation in neat plastic semiconductors *J. Mater. Chem. C* **3** 10715–22

[19] Liu W, Yang X, He D, He L, Li L, Liu Y, Liu J and Wang K 2016 Dopamine modulated ionic permeability in mesoporous silica sphere based biomimetic compartment *Colloids Surfaces B Biointerfaces* **142** 266–71

[20] Aznar E, Oroval M, Pascual L, Murguía J R, Martínez-Máñez R and Sancenón F 2016 Gated Materials for On-Command Release of Guest Molecules *Chem. Rev.* **116** 561–718

[21] Niedermayer S, Weiss V, Herrmann A, Schmidt A, Datz S, Müller K, Wagner E, Bein T and Bräuchle C 2015 Multifunctional polymer-capped mesoporous silica nanoparticles for pH-responsive targeted drug delivery *Nanoscale* **7** 7953–64

[22] Luo Z, Cai K, Hu Y, Zhao L, Liu P, Duan L and Yang W 2011 Mesoporous silica nanoparticles end-capped with collagen: Redox-responsive nanoreservoirs for targeted drug delivery *Angew. Chemie - Int. Ed.* **50** 640–3

[23] Guillet-Nicolas R, Popat A, Bridot J L, Monteith G, Qiao S Z and Kleitz F 2013 PH-responsive nutraceutical-mesoporous silica nanoconjugates with enhanced colloidal stability *Angew. Chemie - Int. Ed.* **52** 2318–22

[24] Sun Y L, Yang B J, Zhang S X A and Yang Y W 2012 Cucurbit[7]uril pseudorotaxane-based photoresponsive supramolecular nanovalve *Chem. - A Eur. J.* **18** 9212–6

[25] Li Q L, Wang L, Qiu X L, Sun Y L, Wang P X, Liu Y, Li F, Qi A Di, Gao H and Yang Y W 2014 Stimuli-responsive biocompatible nanovalves based on β-cyclodextrin

modified poly(glycidyl methacrylate) *Polym. Chem.* **5** 3389–95

[26] Vivero-Escoto J L, Slowing I I, Wu C W and Lin V S Y 2009 Photoinduced intracellular controlled release drug delivery in human cells by gold-capped mesoporous silica nanosphere *J. Am. Chem. Soc.* **131** 3462–3

[27] Muhammad F, Guo M, Qi W, Sun F, Wang A, Guo Y and Zhu G 2011 PH-triggered controlled drug release from mesoporous silica nanoparticles via intracelluar dissolution of ZnO nanolids *J. Am. Chem. Soc.* **133** 8778–81

[28] Gan Q, Lu X, Yuan Y, Qian J, Zhou H, Lu X, Shi J and Liu C 2011 A magnetic, reversible pH-responsive nanogated ensemble based on Fe3O4 nanoparticles-capped mesoporous silica *Biomaterials* **32** 1932–42

[29] Chen P J, Hu S H, Hsiao C S, Chen Y Y, Liu D M and Chen S Y 2011 Multifunctional magnetically removable nanogated lids of Fe 3O4-capped mesoporous silica nanoparticles for intracellular controlled release and MR imaging *J. Mater. Chem.* **21** 2535–43

[30] Alberti S, Soler-Illia G J A A and Azzaroni O 2015 Gated supramolecular chemistry in hybrid mesoporous silica nanoarchitectures: Controlled delivery and molecular transport in response to chemical, physical and biological stimuli *Chem. Commun.* **51** 6050–75

[31] Chen Z, Cui Z, Cao C, He W, Jiang L and Song W 2012 Temperature-Responsive Smart Nanoreactors: Poly(N-isopropylacrylamide)-Coated Au@Mesoporous-Si)2 Hollow Nanospheres *Langmuir* **28** 13452–8

[32] Zhao R, Hu J, Niu C, Li Y, Hu M, Liu R and Li S 2016 A smart nanoreactor with photo-

responsive molecular switches for controlling catalytic reactions *J. Mater. Chem. C* **4** 4748–55

[33] Zhang Y, Ang C Y, Li M, Tan S Y, Qu Q and Luo Z 2015 Polymer Coated Hollow Mesoporous Nanoparticles for Triple-Responsive Delivery Silica Drug *ACS Appl. Mater. Interfaces* **7** 18179–87

[34] Tian B, Liu S, Wu S, Lu W, Wang D, Jin L, Hu B, Li K, Wang Z and Quan Z 2017 pH-responsive poly (acrylic acid)-gated mesoporous silica and its application in oral colon targeted drug delivery for doxorubicin *Colloids Surfaces B Biointerfaces* **154** 287–96

[35] Schlossbauer A, Warncke S, Gramlich P M E, Kecht J, Manetto A, Carell T and Bein T 2010 A programmable DNA-based molecular valve for colloidal mesoporous silica *Angew. Chemie - Int. Ed.* **49** 4734–7

[36] Zhang P, Cheng F, Zhou R, Cao J, Li J, Burda C, Min Q and Zhu J J 2014 DNA-hybrid-gated multifunctional mesoporous silica nanocarriers for dual-targeted and microRNA-responsive controlled drug delivery *Angew. Chemie - Int. Ed.* **53** 2371–5

[37] Bringas E, Köysüren Ö, Quach D V., Mahmoudi M, Aznar E, Roehling J D, Marcos M D, Martínez-Máñez R and Stroeve P 2012 Triggered release in lipid bilayer-capped mesoporous silica nanoparticles containing SPION using an alternating magnetic field *Chem. Commun.* **48** 5647–9

[38] Han N, Zhao Q, Wan L, Wang Y, Gao Y, Wang P, Wang Z, Zhang J, Jiang T and Wang S 2015 Hybrid lipid-capped mesoporous silica for stimuli-responsive drug release and overcoming multidrug resistance *ACS Appl. Mater. Interfaces* **7** 3342–51

[39] Yang J, He W D, He C, Tao J, Chen S Q, Niu S M and Zhu S L 2013 Hollow mesoporous silica nanoparticles modified with coumarin-containing copolymer for photo-modulated loading and releasing guest molecule *J. Polym. Sci. Part A Polym. Chem.* **51** 3791–9

[40] He D, He X, Wang K, Cao J and Zhao Y 2012 A light-responsive reversible molecule-gated system using thymine-modified mesoporous silica nanoparticles *Langmuir* **28** 4003–8

[41] Ferris D P, Zhao Y, Khashab N M, Khatib H A, Stoddart J F and Zink J I 2009 Ja807798G *J. Am. Chem. Soc.* **131** 1686–8

[42] Mei X, Yang S, Chen D, Li N, Li H, Xu Q, Ge J and Lu J 2012 Light-triggered reversible assemblies of azobenzene-containing amphiphilic copolymer with β-cyclodextrin-modified hollow mesoporous silica nanoparticles for controlled drug release *Chem. Commun.* **48** 10010–2

[43] Yi S, Zheng J, Lv P, Zhang D, Zheng X, Zhang Y and Liao R 2018 Controlled Drug Release from Cyclodextrin-Gated Mesoporous Silica Nanoparticles Based on Switchable Host-Guest Interactions *Bioconjug. Chem.* **29** 2884–91

[44] Angelos S, Yang Y W, Patel K, Stoddart J F and Zink J I 2008 pH-responsive supramolecular nanovalves based on cucurbit[6]uril pseudorotaxanes *Angew. Chemie - Int. Ed.* **47** 2222–6

[45] Lee S F, Zhu X M, Wang Y X J, Xuan S H, You Q, Chan W H, Wong C H, Wang F, Yu J C, Cheng C H K and Leung K C F 2013 Ultrasound, pH, and magnetically responsive crown-ether-coated core/shell nanoparticles as drug encapsulation and release systems

ACS Appl. Mater. Interfaces **5** 1566–74

[46] Nguyen T D, Leung K C F, Liong M, Pentecost C D, Stoddart J F and Zink J I 2006 Construction of a pH-driven supramolecular nanovalve *Org. Lett.* **8** 3363–6

[47] Huang X and Du X 2014 Pillar[6]arene-valved mesoporous silica nanovehicles for multiresponsive controlled release *ACS Appl. Mater. Interfaces* **6** 20430–6

[48] Sun Y L, Yang Y W, Chen D X, Wang G, Zhou Y, Wang C Y and Stoddart J F 2013 Mechanized silica nanoparticles based on pillar[5]arenes for on-command cargo release *Small* **9** 3224–9

[49] Liu R, Zhang Y, Zhao X, Agarwal A, Mueller L J and Feng P 2010 pH-responsive nanogated ensemble based on gold-capped mesoporous silica through an acid-labile acetal linker *J. Am. Chem. Soc.* **132** 1500–1

[50] Yang Y, Lin Y, Di D, Zhang X, Wang D, Zhao Q and Wang S 2017 Gold nanoparticle-gated mesoporous silica as redox-triggered drug delivery for chemo-photothermal synergistic therapy *J. Colloid Interface Sci.* **508** 323–31

[51] Lai C Y, Trewyn B G, Jeftinija D M, Jeftinija K, Xu S, Jeftinija S and Lin V S Y 2003 A mesoporous silica nanosphere-based carrier system with chemically removable CdS nanoparticle caps for stimuli-responsive controlled release of neurotransmitters and drug molecules *J. Am. Chem. Soc.* **125** 4451–9

[52] Sparreboom W, Van Den Berg A and Eijkel J C T 2009 Principles and applications of nanofluidic transport *Nat. Nanotechnol.* **4** 713–20

[53] Karnik R, Fan R, Yue M, Li D, Yang P and Majumdar A 2005 Electrostatic control of

ions and molecules in nanofluidic transistors *Nano Lett.* **5** 943–8

[54] Stein D, Kruithof M and Dekker C 2004 Surface-charge-governed ion transport in nanofluidic channels *Phys. Rev. Lett.* **93** 1–4

[55] Austin R H, Tung C, Lambert G and Liao D 2010 From microfluidic application to nanofluidic phenomena issue Reviewing the latest advances in microfluidic and nanofluidic An introduction to micro-ecology patches w *Chem. Soc. Rev.* **39** 1049–59

[56] Li M, Harbron R L, Weaver J V M, Binks B P and Mann S 2013 Electrostatically gated membrane permeability in inorganic protocells *Nat. Chem.* **5** 529–36

[57] Lee C H, Lo L W, Mou C Y and Yang C S 2008 Synthesis and characterization of positive-charge functionalized mesoporous silica nanoparticles for oral drug delivery of an anti-inflammatory drug *Adv. Funct. Mater.* **18** 3283–92

[58] Daiguji H, Yang P, Szeri A J and Majumdar A 2004 Electrochemomechanical energy conversion in nanofluidic channels *Nano Lett.* **4** 2315–21

[59] Kumar B V V S P, Sonu K P, Rao K V, Sampath S, George S J and Eswaramoorthy M 2018 Supramolecular Switching of Ion-Transport in Nanochannels *ACS Appl. Mater. Interfaces* **10** 23458–65

[60] Brunsen A, Díaz C, Pietrasanta L I, Yameen B, Ceolín M, Soler-Illia G J A A and Azzaroni O 2012 Proton and calcium-gated ionic mesochannels: Phosphate-bearing polymer brushes hosted in mesoporous thin films as biomimetic interfacial architectures *Langmuir* **28** 3583–92

[61] Yameen B, Ali M, Neumann R, Ensinger W, Knoll W and Azzaroni O 2009 Single

conical nanopores displaying pH-tunable rectifying characteristics. manipulating ionic transport with zwitterionic polymer brushes *J. Am. Chem. Soc.* **131** 2070–1

[62] Lee S B and Martin C R 2001 Membrane Based on Chemisorbed Cysteine *Anal. Chem.* **73** 768–75

[63] Ali M, Ramirez P, Mafé S, Neumann R and Ensinger W 2009 A pH-Tunable nanofluidic diode with a broad range of rectifying properties *ACS Nano* **3** 603–8

[64] Brunsen A, Cui J, Ceolín M, Campo A Del, Soler-Illia G J A A and Azzaroni O 2012 Light-activated gating and permselectivity in interfacial architectures combining “caged” polymer brushes and mesoporous thin films *Chem. Commun.* **48** 1422–4

[65] Wen L, Liu Q, Ma J, Tian Y, Li C, Bo Z and Jiang L 2012 Malachite green derivative-functionalized single nanochannel: Light-and-pH dual-driven ionic gating *Adv. Mater.* **24** 6193–8

[66] Wang G, Bohaty A K, Zharov I and White H S 2006 Photon gated transport at the glass nanopore electrode *J. Am. Chem. Soc.* **128** 13553–8

[67] Elbert J, Krohm F, Rüttiger C, Kienle S, Didzoleit H, Balzer B N, Hugel T, Stühn B, Gallei M and Brunsen A 2014 Polymer-modified mesoporous silica thin films for redox-mediated selective membrane gating *Adv. Funct. Mater.* **24** 1591–601

[68] Matthews J R, Tuncel D, Jacobs R M J, Bain C D and Anderson H L 2003 Surfaces designed for charge reversal *J. Am. Chem. Soc.* **125** 6428–33

[69] Wang Y, Sun Y, Wang J, Yang Y, Li Y, Yuan Y and Liu C 2016 Charge-Reversal APTES-Modified Mesoporous Silica Nanoparticles with High Drug Loading and Release

Controllability *ACS Appl. Mater. Interfaces* **8** 17166–75

[70] Fattakhova-Rohlfing D, Wark M and Rathouský J 2007 Ion-permselective pH-switchable mesoporous silica thin layers *Chem. Mater.* **19** 1640–7

[71] Kumar B V V S P, Salikolimi K and Eswaramoorthy M 2014 Glucose- and pH-Responsive Charge-Reversal Surfaces *Langmuir* **30** 4540–4

[72] Balamurali V, Pramodkuma T M, Srujana N, Venkatesh M P, Gupta N V, Krishna K L and Gangadhara H V 2010 pH Sensitive Drug Delivery Systems: A Review *Am. J. Drug Discov. Dev.* **1** 24–48

[73] Yang Q, Wang S, Fan P, Wang L, Di Y, Lin K and Xiao F S 2005 pH-responsive carrier system based on carboxylic acid modified mesoporous silica and polyelectrolyte for drug delivery *Chem. Mater.* **17** 5999–6003

[74] Gu Y J, Cheng J, Jin J, Cheng S H and Wong W T 2011 Development and evaluation of pH-responsive single-walled carbon nanotube-doxorubicin complexes in cancer cells. *Int. J. Nanomedicine* **6** 2889–98

[75] Zhu J, Liao L, Bian X, Kong J, Yang P and Liu B 2012 PH-controlled delivery of doxorubicin to cancer cells, based on small mesoporous carbon nanospheres *Small* **8** 2715–20

[76] Li M, Zhang C, Yang X L and Xu H B 2013 Microfluidization-assisted synthesis of hollow mesoporous silica nanoparticles *J. Sol-Gel Sci. Technol.* **67** 501–6

[77] Ma X, Zhao Y, Ng K W and Zhao Y 2013 Integrated hollow mesoporous silica nanoparticles for target drug/siRNA co-delivery *Chem. - A Eur. J.* **19** 15593–603

[78] Huh S, Wiench J W, Yoo J C, Pruski M and Lin V S Y 2003 Organic Functionalization and Morphology Control of Mesoporous Silicas via a Co-Condensation Synthesis Method *Chem. Mater.* **15** 4247–56

[79] Dias D R, Moreira A F and Correia I J 2016 The effect of the shape of gold core-mesoporous silica shell nanoparticles on the cellular behavior and tumor spheroid penetration *J. Mater. Chem. B* **4** 7630–40

[80] Dai L, Li J, Zhang B, Liu J, Luo Z and Cai K 2014 Redox-responsive nanocarrier based on heparin end-capped mesoporous silica nanoparticles for targeted tumor therapy in vitro and in vivo *Langmuir* **30** 7867–77

[81] Fisk J D, Batten R, Jones G, O'Reilly J P and Shaw A M 2005 pH Dependence of the crystal violet adsorption isotherm at the silica-water interface *J. Phys. Chem. B* **109** 14475–80

[82] Manzo V, Navarro O, Honda L, Sánchez K, Toral M I and Richter P 2013 Determination of crystal violet in water by direct solid phase spectrophotometry after rotating disk sorptive extraction *Talanta* **106** 305–8